Physics – Uspekhi **58** (2) 107 – 133 (2015)

REVIEWS OF TOPICAL PROBLEMS PACS numbers: **52.35. – g**, 94.30.cq, 94.30.ct

Discontinuous plasma flows in magnetohydrodynamics and in the physics of magnetic reconnection

L S Ledentsov, B V Somov

DOI: 10.3367/UFNe.0185.201502a.0113

Contents

Abstract. We review the current status of the theory of discontinuous magnetohydrodynamic (MHD) flows and its application to the physics of magnetic reconnection in astrophysical plasmas and in laboratory and numerical simulation studies. The emphasis is on the study of continuous transitions occurring between different types of discontinuities under gradual and continuous variation of the plasma flow parameters. The properties of the Syrovatskii reconnecting current sheet are described, and the possibility of the splitting of the current sheet into a system of MHD discontinuities is demonstrated. A simplified analytic model of magnetic reconnection is used to study the system of shock waves associated with the current sheet. With this system as an example, some implications of the conditions of continuous transitions and the possibility of additional plasma heating by a shock wave are considered.

Keywords: magnetic reconnection, plasma, MHD discontinuities

L S Ledentsov, B V Somov Lomonosov Moscow State University, Sternberg Astronomical Institute,
Universitetskii prosp. 13, 119991 Moscow, Russian Federation
E-mail: koob@mail.ru, somov@sai.msu.ru

Received 1 June 2014, revised 15 July 2014
Uspekhi Fizicheskikh Nauk **185** (2) 113 – 142 (2015)
DOI: 10.3367/UFNr.0185.201502a.0113
Translated by K A Postnov; edited by A M Semikhatov

1. Introduction

Magnetohydrodynamics (MHD) describes the behavior of a conducting medium (liquid or gaseous) interacting with an electromagnetic field. The MHD theory is based on the electromagnetic field and fluid dynamics equations. Progress in MHD studies peaked in the middle of the 20th century and was related (in addition to numerous technical applications) to new problems in solar physics, geophysics, and astrophysics. This was due to specific features of the objects, first of all, the high ionization degree of the interstellar gas, stellar atmospheres, and stellar interiors, which makes these media excellent conductors. Second, magnetic fields have an energy density comparable to that of the surrounding medium, i.e., they can control frozen plasma flows. Third, the large scales of space objects justify their hydrodynamic description.

The basics of MHD were formulated in the 1940s by the Swedish physicist H Alfvén, who proposed this theory to explain some phenomena in space plasma [1]. Alfvén described a new type of wave motion of a conducting medium in the magnetic field — magnetohydrodynamic waves, now known as Alfvén waves. Later, several more characteristic low-amplitude waves in magnetized media were identified, such as fast and slow magnetosonic waves.

Unlike Alfvén and magnetosonic waves, which are described by small perturbations in the equations for

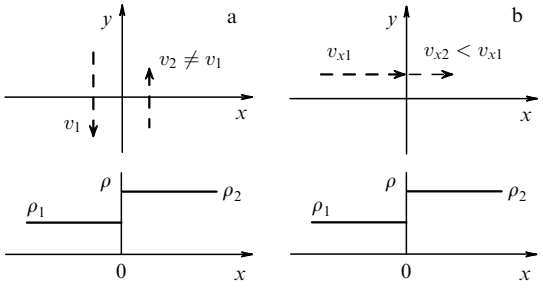

Figure 1. Hydrodynamic discontinuous flows: (a) tangential discontinuity, (b) shock wave.

conducting media, discontinuous flows are regions where solutions of nonlinear equations for two continuous fluids separated by a discontinuity surface are to be matched. Complex interactions of the magnetic field with matter in MHD (especially when a high-temperature plasma in a strong magnetic field is considered) give rise to many different discontinuous solutions [2].

We recall that a drastic change (jump) in the parameters of matter occurs across the discontinuity surface. As is well known, equations of ordinary fluid dynamics allow discontinuous solutions of two types: tangential discontinuities and shocks [3]. The first solution is an interface between two media moving relative to each other; there is no matter flow through the discontinuity from one medium into another. In a shock, by contrast, the matter inflows into the discontinuity supersonically and outflows from it subsonically. This property of shocks provides their mechanical stability. Small perturbations propagate only with the speed of sound and are unable to cross the shock front, which is conducive to keeping the sharp form of the front. Figure 1 illustrates both types of hydrodynamic discontinuities in a reference frame co-moving with the discontinuity along the x axis directed normally to the discontinuity surface.

In MHD, the presence of a magnetic field in a plasma leads to the formation of fast and slow shocks, Alfvén flows, and other discontinuities [4–6]. The discontinuous MHD flow type is determined by changes in the plasma density, its flow velocity, and the frozen magnetic field strength. Moreover, unlike fluid dynamics, MHD allows continuous transitions between different types of discontinuities under continuous changes in the plasma flow conditions [7]. This proceeds via the so-called transition solutions, which satisfy two types of discontinuity conditions simultaneously. In addition, on the discontinuity surface, plasma heating occurs, which, of course, also depends on the MHD discontinuity type, but does not determine its classification pattern, namely, the continuity or jump of the density or the presence or absence of the normal velocity component $v_\perp$ and the normal magnetic field $B_\perp$.

The possibility of transitions between discontinuities of different types can be conveniently represented as a block diagram in which each block corresponds to a particular MHD flow type. Several such diagrams have been proposed at different times [7–9]. Each subsequent diagram included more diverse MHD discontinuities than the previous one. Such diagrams, taking all possible types of discontinuities into account and describing the allowed transitions between them, are necessary, for example, in order to interpret modern numerical simulations of the magnetic reconnection.

Discontinuous plasma flows can be realized under a wide range of physical conditions. As a consequence, they occur in various technological devices and setups used in practice (see [10–12]), in laboratory and numerical experiments (see, e.g., [13–15]), and in space conditions [16–18], especially in relation to the magnetic reconnection effect [19–23]. This effect is a rearrangement of the interacting magnetic fluxes that changes their topological connection. Typically, the interaction of magnetic fluxes in a highly conducting plasma, for example, in the solar corona, generates electric currents, more precisely, thin current surfaces or current sheets, which can be considered two-dimensional discontinuous MHD flows [24–26].

In highly conducting plasmas, current sheets significantly slow down the reconnection process compared to the vacuum case. A substantial magnetic energy excess is stored in the magnetic field of the current sheets, which corresponds to the interaction energy of nonreconnected magnetic fluxes and is called the free magnetic energy. For a current sheet in the solar corona, the free energy can be as high as 10^{32} erg, which corresponds to the energy of the most powerful solar flares. Thus, Syrovatskii's theory of current sheets [27] answered the key questions of the physics of solar flares: where, when, and in which form is their energy accumulated.

The second important feature of the Syrovatskii current sheet is its metastability. It is stable only in a certain range of physical parameters. Depending on their values, the current sheet either is stable and slowly changes with variations of the parameters, or loses stability at some threshold values of the parameters, which leads to a rapid dissipation of the stored energy in the form of a solar flare [28].

Omitting significant details and stages of the development of a solar flare, we only note that the fast magnetic reconnection in the flare occurs in a high-temperature turbulent current sheet [29, 30]. During the flare, the reconnection rapidly transforms the magnetic field energy stored before the flare into the energy of plasma particles. A significant fraction of the flare energy is then released in the form of jets — high-velocity narrow plasma flows from the current sheet. Outside the current sheet, the jets give rise to a complex picture of discontinuous MHD flows. Understanding this picture is necessary, in particular, for explaining observational properties of powerful eruptive flares, coronal mass ejections, and other geoeffective solar phenomena [31–33].

X-ray space observatories, the international Yokoh satellite first of all [34, 35], allowed observing consequences of the magnetic reconnection in solar flares. The most pronounced among them are the so-called solar flare loops observed in soft X-rays [36, 37]. The motion of the loop base, observed in hard X-rays [34, 36], directly evidences the magnetic reconnection at the magnetic field separatrices in the solar corona. Other manifestations of the magnetic reconnection include the high-temperature plasma rising from the chromosphere to the corona along the reconnecting field lines [36], hard X-ray sources at the top of the loops [38, 39], horizontal motion of matter in the reconnecting region [40], plasma flows [41], and whole plasma 'islands' injected with high velocity from the solar corona into the interplanetary space [42, 43].

In the last decade, detailed images from the space observatories RHESSI and SDO have resolved the double structure of the hard X-ray emission above the solar flare loop tops [44, 45]. The coronal source of the hard X-ray

emission is directly related to the plasma heated and accelerated at opposite ends of the current sheet. The measured spectra and temperature profiles of this emission depend on the local magnetic field configuration and plasma density [46]. Observations suggest that the jet formation regions and shocks play a significant role in particle acceleration and plasma heating to huge temperatures [47]. Despite these data, so far no direct observations of the formation and evolution of a current sheet in a flare have been obtained. A high electric conductivity and an almost force-free configuration of the magnetic field restrict the reconnecting current sheet to a very narrow region in the rarefied corona, which makes the sheet difficult to observe due to a very small proper emission.

Modern numerical simulations of the magnetic reconnection (both two- and three-dimensional) in the dissipative MHD approximation demonstrate a somewhat smoothed picture of discontinuous flows in the vicinity of a reconnecting current sheet [48–52]. When interpreting the results of such simulations, especially in 3D, it is difficult to uniquely identify the type of the discontinuity using an incomplete set of features. Once this difficulty is overcome, a second problem arises: it is necessary to explain the simultaneous presence of different discontinuity types, which smoothly transit from one into another.

The problem of interpretation of the continuous transitions is frequently complicated by the emergence of nonevolutionary discontinuities [53]. Small perturbations applied to the surface of a nonevolutionary discontinuity instantly lead to big changes in the discontinuous flow. This distinctive property of nonevolutionarity is different from instability: the usual instability is related to a gradual increase in small perturbations that remain small during some finite time interval. But in a nonevolutionary discontinuity, perturbations become large immediately. For this reason, the detection and analysis of nonevolutionary regions are important tasks of the fluid dynamics and MHD. These features are especially difficult to observe in numerical simulations of the magnetic reconnection process.

In [53, 54], a two-dimensional stationary model of reconnection in a strong magnetic field was considered, including a Syrovatskii-type thin current sheet [26] and four finite-length discontinuous MHD flows attached to its edges [56]. The analytic solution of the problem allows constructing the pattern of magnetic field lines around the reconnection location. The calculated field structure is generally very complicated. The formation of the current sheet is accompanied by reverse currents arising at its edges, which makes this structure nonevolutionary [57, 58]. Explaining the structure and comparing it with numerical simulations, for example, those carried out in the dissipative MHD approximation [59–63], requires a simple and convenient interpretation of the magnetic field structure change on the discontinuity surface in the 'laboratory' frame with a nonzero electric field, which inevitably arises during magnetic reconnection.

We here review the properties of discontinuous MHD flows and the magnetic reconnection physics. In Section 2, we consider the boundary conditions of the ideal MHD on the discontinuity surface. An equation that relates the magnetic field line inclination angles at different sides of a two-dimensional discontinuous flow is derived. Using the characteristic parameter, namely, the mass flow rate across the discontinuity, the relation of this dependence to the standard MHD plasma flow classification is obtained.

In Section 3, we seek the transition solutions between all neighboring pairs of the MHD discontinuities among both 2D- and 3D-flows. Section 4 is devoted to the study of a boundary condition that is equivalent to the energy conservation at the discontinuity surface. The corresponding equation does not reflect the classification pattern of the discontinuity, but bears information about the plasma internal energy and hence about the ability of an MHD flow to heat the plasma. We seek an equation that explicitly describes the plasma internal energy change across the discontinuity. The dependence of this equation on both thermodynamic parameters of the medium and the MHD discontinuity type is examined.

The basic properties of the Syrovatskii reconnecting current sheet are described in Section 5; here, the notion of evolutionarity is introduced. Typical approximations are considered that allow addressing the evolutionarity of the current sheet as a discontinuous MHD flow. In Section 6, we study the evolutionarity of a reconnecting current sheet. The fundamental possibility of the current sheet splitting into a system of MHD discontinuities is demonstrated.

Properties of discontinuous flows near a reconnecting current sheet in a strong magnetic field are discussed in Section 7. A self-consistent analytic model of the magnetic field is considered in the strong-field and cold-plasma approximation. MHD flows that are formed at the side edges of the reconnecting current sheet are classified. It is shown that the magnetic field configuration changes with the distance from the current sheet, signaling a change in the discontinuous flow type. The analysis of the corresponding transition solutions confirms the possibility of additional plasma heating by shocks outside the reconnection domain. Conclusions are formulated in Section 8.

2. Magnetic field change at the magnetohydrodynamic discontinuity

2.1 Boundary conditions at the discontinuity

In the vicinity of an MHD discontinuity, the plasma density, its pressure, the flow velocity, and the direction and strength of the magnetic field can change abruptly over a scale comparable to the mean free path of particles. Physical processes inside such a jump are determined by kinetic phenomena in the plasma, both laminar and turbulent [64]. In the dissipative MHD approximation, the internal structure of a discontinuous plasma flow is determined by the dissipative transport coefficients (viscosity and electric conductivity) as well as by the heat conductivity [65, 66]. However, in the ideal MHD approximation, this jump has zero thickness, i.e., it occurs on some discontinuity surface.

We consider a flat discontinuity surface, which is relevant for areas whose diameter is small compared to the surface curvature radius. Figure 2 shows the reference frame in which the observer moves together with the discontinuity surface located in the plane (y, z). The homogeneous plasma inflows with a constant velocity into the discontinuity from the left-hand side and outflows from it to the right. In the ideal MHD approximation, we neglect the viscosity, thermal conductivity, and electric conductivity of the plasma. Then the boundary conditions for the MHD equations at the discontinuity can be written in the form of the conservation

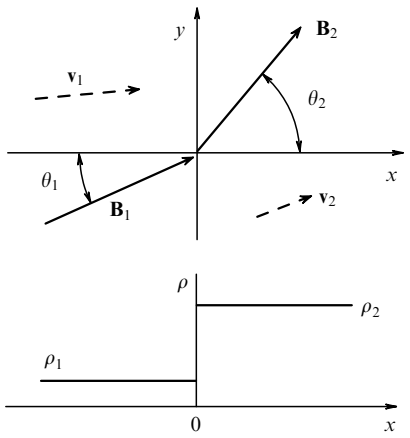

Figure 2. Change in the magnetic field **B**, velocity field **v**, and plasma density ρ at the shock front $x = 0$.

laws [4, 67, 68]

$$\{B_x\} = 0\,, \tag{1}$$

$$\{\rho v_x\} = 0\,, \tag{2}$$

$$\{v_x B_y - v_y B_x\} = 0\,, \tag{3}$$

$$\{v_x B_z - v_z B_x\} = 0\,, \tag{4}$$

$$\left\{\rho v_x v_y - \frac{1}{4\pi} B_x B_y\right\} = 0\,, \tag{5}$$

$$\left\{\rho v_x v_z - \frac{1}{4\pi} B_x B_z\right\} = 0\,, \tag{6}$$

$$\left\{p + \rho v_x^2 + \frac{B^2}{8\pi}\right\} = 0\,, \tag{7}$$

$$\left\{\rho v_x\left(\frac{v^2}{2} + \epsilon + \frac{p}{\rho}\right) + \frac{1}{4\pi}\left(B^2 v_x - (\mathbf{vB})B_x\right)\right\} = 0\,. \tag{8}$$

We use the standard notation for the physical quantities, unless stated otherwise. Curly brackets denote the difference in the values of the expressions inside them on each side of the discontinuity. For example, the first equation implies the continuity of the normal component of the magnetic field:

$$\{B_x\} = B_{x2} - B_{x1} = 0\,,$$

or, equivalently, the magnetic flux conservation. The other seven equations also bear a simple physical meaning: Eqn (2) expresses the mass flux continuity; Eqns (3) and (4) are conditions of the continuity of the tangential electric field component; Eqns (5)–(7) describe the continuity of the three momentum flux components; finally, Eqn (8) is the condition of the energy flux continuity. Quantities with the index 1 are related to the left-hand side of Fig. 2, corresponding to the upstream plasma, and those with the index 2, to the right-hand side of Fig. 2, corresponding to the downstream plasma. Of course, in addition to these eight equations, the plasma equation of state is assumed to be known, for example, in the form of the specific (per unit mass) enthalpy w as a function of the density ρ and pressure p.

As is well known, the system of boundary conditions (1)–(8), unlike a similar system in hydrodynamics, does not decompose into a set of mutually incompatible groups of equations, and therefore, in principle, allows continuous transitions between different types of discontinuous flows under continuous changes in the plasma flow conditions. Hydrodynamic discontinuous flows can be of only two types [tangential discontinuities and shocks (see Fig. 1)] and can have only two propagation velocities (zero and the speed of sound, respectively). This property prohibits continuous transitions between hydrodynamic flows. Transitions in MHD occur through some discontinuities, which simultaneously satisfy the boundary conditions for two adjacent types of discontinuous flows, and can therefore be related to one type or another [7]. The existence of such transitions can be guessed by passing from the discontinuous solutions to the limit of low-amplitude waves and studying their phase velocity diagrams [29, 69]. In this limit, the fast and slow magnetosonic waves correspond to oblique shocks, and the rotational discontinuity corresponds to the Alfvén wave.

If there are transition solutions, the classification of MHD discontinuities becomes conventional. Indeed, a discontinuity of a certain type can continuously transform into a discontinuity of another type under a smooth change in the incident plasma parameters. As we show in Section 4, the discontinuity type can change from one point to another on the discontinuity surface. In any case, due to the possibility of smooth transitions between discontinuities of different types, their classification is based on the local *external properties* of the flow near the discontinuity plane, including the presence or absence of the normal components of the velocity v_x and the magnetic field B_x (those perpendicular to the plane), the continuity or a jump in the density ρ. Relative to these signatures, the energy conservation law (8) is an additional condition: with the magnetic field, the velocity field, and the density jump found, Eqn (8) determines the jump in the internal energy ϵ.

Before seeking transition solutions, we must understand under what conditions different types of discontinuities are formed. Without loss of generality, we rotate the coordinate system about the x axis such that the velocity component vanishes, $v_{z1} = 0$. Then, substituting (1) in (6) and using (2), we obtain the equation

$$\frac{B_x}{4\pi}\{B_z\} = \rho v_x v_{z2}\,. \tag{9}$$

We consider some simple particular solutions of this equation (Fig. 3):

(1) If $B_x = 0$ and $v_x = 0$, i.e., the magnetic field does not cross the discontinuity and the plasma does not flow through it, Eqn (9) implies that $\{B_z\}$ and v_{z2} can take arbitrary values. Relations (3) and (5) also suggest the arbitrariness of $\{v_y\}$ and $\{B_y\}$. Equation (7) implies that the pressure and magnetic field strength are related by the total pressure continuity condition:

$$\left\{p + \frac{B^2}{8\pi}\right\} = 0\,.$$

This solution corresponds to the classical tangential discontinuity (Fig. 3a).

(2) If $B_x = 0$ but $v_x \neq 0$ [which together with (9) then implies that $v_z = 0$], the magnetic field is parallel to the discontinuity plane and, as can be seen from (2)–(4), changes due to the plasma flow across the discontinuity and its compression in accordance with the magnetic flux freezing condition:

$$\left\{\frac{\mathbf{B}}{\rho}\right\} = 0\,.$$

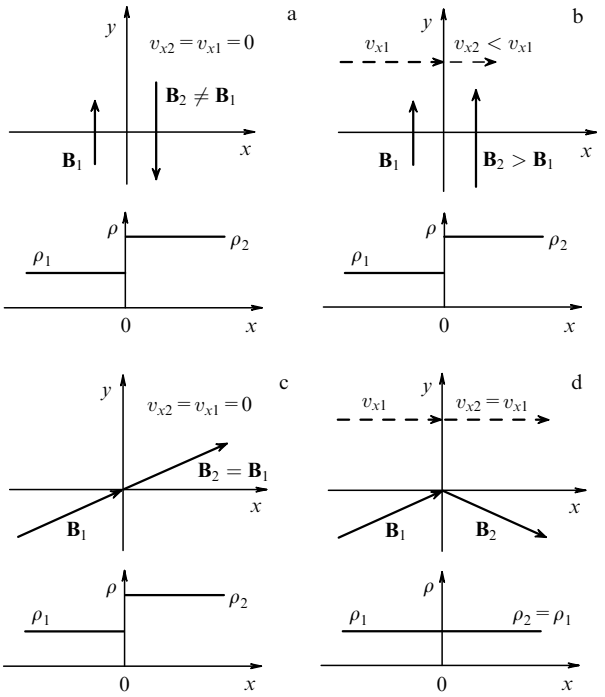

Figure 3. Schematics of discontinuities projected on the (x, y) plane: (a) tangential discontinuity, (b) perpendicular shock, (c) contact discontinuity, (d) Alfvén shock.

This type of discontinuity corresponds to a perpendicular shock (Fig. 3b), which is also well known in MHD. It represents a usual compression wave propagating perpendicularly to the magnetic field direction and compressing the plasma together with the frozen magnetic flux.

(3) Let $B_x \neq 0$ and $v_x = 0$ [and hence, according to (9), $\{B_z\} = 0$]; then Eqns (3)–(5) imply the continuity of the components v_y, v_z, and B_y. The magnetic field direction does not change across the discontinuity, but the density can change. This is a contact discontinuity (Fig. 3c).

(4) If both $B_x \neq 0$ and $v_x \neq 0$, substituting $v_z = 0$ in (9) yields $\{B_z\} = 0$. As a result, Eqn (4) becomes

$$B_z\{v_x\} = 0\,.$$

This equation, naturally, has two different solutions.

(a) We first consider the solution $\{v_x\} = 0$. Substituting this solution in (2) yields a new condition $\{\rho\} = 0$, which in the presence of a plasma flow across the plane (with $v_x \neq 0$) corresponds to an Alfvén shock. Using the condition $\{B_z\} = 0$ and assuming that $\{p\} = 0$ due to all other thermodynamic quantities being zero, we rewrite Eqn (7) in the form $\{B_y^2\} = 0$. If $\{B_y\} = 0$, no changes occur in the medium and there is no discontinuity. Therefore, $B_{y2} = -B_{y1}$ (Fig. 3d).

(b) The solution $B_z = 0$ leads to a two-dimensional picture of the discontinuity: the velocity and magnetic field vectors lie in one plane normal to the discontinuity plane (see Fig. 2).

Thus, the presence or absence of the plasma flow and the magnetic field penetration through the discontinuity surface allow identifying the discontinuity type (see a more detailed discussion of the discontinuity properties, e.g., in [7, 69]). The description of many discontinuous flows is significantly simplified in the so-called de Hoffmann–Teller frame. This frame is moving along the discontinuity surface with the velocity

$$\mathbf{u}_{\mathrm{HT}} = \mathbf{v} - \frac{v_x}{B_x}\,\mathbf{B}\,,$$

and therefore the vectors $\mathbf{v}$ and $\mathbf{B}$ become parallel to each other. In particular, the Alfvén discontinuity is then described as the magnetic field strength vector rotated through some angle about the x axis, keeping its modulus constant, and all discontinuous flows (with the magnetic field inclined to the discontinuity plane) turn out to be two-dimensional. Due to the constraint $B_x \neq 0$, the de Hoffmann–Teller frame is inapplicable to tangential discontinuities and perpendicular shocks, and we do not discuss it.

However, because all discontinuous flows, except tangential and Alfvén discontinuities and perpendicular shocks, can be reduced to the two-dimensional form, we start by considering the boundary conditions for the two-dimensional case. In Section 2.2 below, in order to find the characteristic parameter that would allow segregating some cases of two-dimensional discontinuous flows, we consider the case referred to as 4 (b) above in more detail.

Hereafter and until Section 4, we study only classification signatures of discontinuous flows, and therefore there is no need in Eqn (8). In this approach, two-dimensional discontinuous flows with $v_z = 0$ and $B_z = 0$ are described by five boundary conditions:

$$\begin{gathered}\{B_x\} = 0\,, \quad \{\rho v_x\} = 0\,, \quad \left\{\rho v_x v_y - \frac{B_x B_y}{4\pi}\right\} = 0\,, \\ \{v_x B_y - v_y B_x\} = 0\,, \quad \left\{\rho v_x^2 + p + \frac{B_y^2}{8\pi}\right\} = 0\,.\end{gathered} \tag{10}$$

We use these equations in Section 2.2 to study the change in the magnetic field at the discontinuity.

2.2 Inclination of magnetic field lines

Two-dimensional discontinuous flows are classified by the behavior of the velocity field and the magnetic field near the discontinuity surface under certain assumptions about the density jump. As in the ideal MHD, the plasma flow velocity is related to the magnetic field by the flux freezing condition; the classification can be based on how the magnetic field changes across the discontinuity. This change can be described by the angles between the magnetic field line (more precisely, the tangent to the magnetic field line at a given point of the discontinuity if the magnetic field lines have some curvature) and the left (upstream) and right (downstream) normals to the discontinuity (see Fig. 2). We refer to these angles as the magnetic field inclination angles. On different sides of the discontinuity, these angles are generally different. To find a convenient parameter characterizing the discontinuous flow type, we first find the relation between these two angles. For this, it is necessary to find the relation between the tangential magnetic field components from boundary conditions (10) and then, using condition (1), to pass to the inclination angle tangents.

Following [70], we introduce new variables $r = 1/\rho$ and $m = \rho v_x$ and rewrite system of equations (10) in the linear form with respect to the jumps $\{v_x\}$, $\{v_y\}$, $\{r\}$, and $\{B_y\}$. To do this, we substitute the first equation in (10) in the third and fourth equation, and pull the quantities that are conserved across the discontinuity outside the curly brack-

ets. We obtain

$$\{v_x\} - m\{r\} = 0\,, \quad m\{v_y\} - \frac{B_x}{4\pi}\,\{B_y\} = 0\,,$$
$$\tilde{B}_y\{v_x\} - B_x\{v_y\} + m\tilde{r}\{B_y\} = 0\,, \tag{11}$$
$$m\{v_x\} + \{p\} + \frac{\tilde{B}_y}{4\pi}\,\{B_y\} = 0\,.$$

Here and hereafter, the tilde denotes mean values, in particular, $\tilde{r} = (r_1 + r_2)/2$.

For nontrivial solutions of the linear system of equations (11) to exist, the determinant of its coefficients must vanish:

$$\begin{vmatrix} -1 & 0 & m & 0 \\ 0 & m & 0 & -\dfrac{B_x}{4\pi} \\ \tilde{B}_y & -B_x & 0 & m\tilde{r} \\ m & 0 & \dfrac{\{p\}}{\{r\}} & \dfrac{\tilde{B}_y}{4\pi} \end{vmatrix} = 0\,.$$

We expand the determinant to obtain

$$\frac{\{p\}}{\{r\}}\left(\frac{B_x^2}{4\pi} - m^2 r\right) + m^2\left(\frac{B_x^2}{4\pi} + \frac{\tilde{B}_y^2}{4\pi} - m^2 r\right) = 0\,.$$

Because m^2 cannot be negative, the last equation imposes a constraint on the admissible mass flux value m:

$$m^2 = -\frac{\{p\}}{\{r\}}\,\frac{m^2 - B_x^2/4\pi\tilde{r}}{m^2 - (B_x^2 + \tilde{B}_y^2)/4\pi\tilde{r}}\,. \tag{12}$$

By the Zemplén MHD theorem (see, e.g., [66])

$$\{r\} = \frac{1}{\rho_2} - \frac{1}{\rho_1} = \frac{\rho_1 - \rho_2}{\rho_1\,\rho_2} < 0\,,$$

and because the pressure p increases with the density ρ for most real substances, one of the following inequalities should be satisfied:

$$m^2 < \frac{B_x^2}{4\pi\tilde{r}} \tag{13}$$

or

$$m^2 > \frac{B_x^2 + \tilde{B}_y^2}{4\pi\tilde{r}}\,. \tag{14}$$

We find the fundamental system of solutions of linear equations (11). The basis minor

$$\begin{vmatrix} -1 & 0 & m \\ 0 & m & 0 \\ \tilde{B}_y & -B_x & 0 \end{vmatrix} \neq 0$$

determines three linearly independent equations:

$$mC_3 = C_1\,, \qquad mC_2 = \frac{B_x}{4\pi}\,C_4\,,$$
$$\tilde{B}_y C_1 - B_x C_2 = -m\tilde{r}C_4\,.$$

Hence,

$$C_1 = \frac{1}{\tilde{B}_y}\left(\frac{B_x^2}{4\pi m} - m\tilde{r}\right)C_4\,,$$
$$C_2 = \frac{B_x}{4\pi m}\,C_4\,,$$
$$C_3 = \frac{1}{m\tilde{B}_y}\left(\frac{B_x^2}{4\pi m} - m\tilde{r}\right)C_4\,.$$

Thus, the solution of system of equations (11) has the form

$$\{v_x\} = C_4\,\frac{1}{\tilde{B}_y}\left(\frac{B_x^2}{4\pi m} - m\tilde{r}\right),$$
$$\{v_y\} = C_4\,\frac{B_x}{4\pi m}\,,$$
$$\{r\} = C_4\,\frac{1}{m\tilde{B}_y}\left(\frac{B_x^2}{4\pi m} - m\tilde{r}\right), \qquad \{B_y\} = C_4\,.$$

Finally, we find

$$\{v_x\} = Cm\left(\frac{B_x^2}{4\pi} - m^2\tilde{r}\right),$$
$$\{v_y\} = Cm\,\frac{B_x\tilde{B}_y}{4\pi}\,,$$
$$\{r\} = C\left(\frac{B_x^2}{4\pi} - m^2\tilde{r}\right), \tag{15}$$
$$\{B_y\} = Cm^2\tilde{B}_y\,.$$

The constant C can be found by substituting the obtained expressions for $\{v_x\}$ and $\{B_y\}$ in the equation for the x-component of the momentum flux from system (11):

$$C = -\frac{\{p\}}{m^2}\left(\frac{B_x^2 + \tilde{B}_y^2}{4\pi} - m^2\tilde{r}\right)^{-1}.$$

We consider the last two equations of system (15). After eliminating the constant C, we find a relation between tangential magnetic field components:

$$\{B_y\} = \frac{m^2\{r\}}{B_x^2/4\pi - m^2\tilde{r}}\,\tilde{B}_y\,.$$

Next, expanding the relations

$$\{B_y\} = B_{y2} - B_{y1}\,,$$
$$\tilde{B}_y = \frac{1}{2}(B_{y2} + B_{y1})\,,$$

we obtain

$$B_{y2} = \frac{2(B_x^2/4\pi - m^2\tilde{r}) + m^2\{r\}}{2(B_x^2/4\pi - m^2\tilde{r}) - m^2\{r\}}\,B_{y1}\,. \tag{16}$$

We divide both sides of (16) by B_x to find the sought relation between the magnetic field inclination angles at different sides of the discontinuity:

$$\tan\theta_2 = \frac{2(B_x^2/4\pi - m^2\tilde{r}) + m^2\{r\}}{2(B_x^2/4\pi - m^2\tilde{r}) - m^2\{r\}}\,\tan\theta_1\,. \tag{17}$$

We next rewrite this equation, by similarly expanding the jumps $\{r\}$ and the mean values $\tilde{r}$:

$$\tan\theta_2 = \frac{m^2\,4\pi r_1/B_x^2 - 1}{m^2\,4\pi r_2/B_x^2 - 1}\tan\theta_1 .$$

We introduce the notation

$$m_{\text{off}}^2 = \frac{B_x^2}{4\pi r_1}, \qquad m_{\text{on}}^2 = \frac{B_x^2}{4\pi r_2} .$$

Below, we show that m_{off} and m_{on} are the respective mass fluxes through the switch-off and switch-on shocks. We note that $m_{\text{off}} \leqslant m_{\text{on}}$ because, according to the Zemplén theorem [66], $r_2 \leqslant r_1$ at the discontinuity. The equation relating the magnetic field inclination angles takes the simple form

$$\tan\theta_2 = \frac{m^2/m_{\text{off}}^2 - 1}{m^2/m_{\text{on}}^2 - 1}\tan\theta_1 . \tag{18}$$

We now introduce the notations

$$m_{\text{A}}^2 = \frac{B_x^2}{4\pi\tilde{r}}, \qquad m_{\perp}^2 = \frac{\tilde{B}_y^2}{4\pi\tilde{r}}$$

to simplify the form of conditions (14) and (13):

$$m^2 < m_{\text{A}}^2 , \tag{19}$$

$$m^2 > m_{\text{A}}^2 + m_{\perp}^2 . \tag{20}$$

The values of m_{off}, m_{A}, and m_{on} resemble those for a plasma flow moving with the Alfvén velocity $V_{\text{A}} = B_x/\sqrt{4\pi\rho}$ and, indeed, become such if $\rho_1 = \rho_2$. As $m \to m_{\text{A}}$, the sign of the tangential component of the magnetic field is reversed. The magnetic field lines have the same configuration at the flat (two-dimensional) Alfvén discontinuity if the magnetic field vector outside the discontinuity plane rotates about the x axis through the angle π. As $m \to m_{\text{A}}$, the conditions for the transitions to the Alfvén discontinuity are established. Because $r_2 \leqslant \tilde{r} \leqslant r_1$,

$$m_{\text{off}} \leqslant m_{\text{A}} \leqslant m_{\text{on}} . \tag{21}$$

We note that the values of m_{off}, m_{A}, and m_{on} are not independent but are related by the condition

$$m_{\text{A}}^2 = \frac{2\,m_{\text{on}}^2\,m_{\text{off}}^2}{m_{\text{on}}^2 + m_{\text{off}}^2} . \tag{22}$$

To see this, we expand the mean value $\tilde{r}$ and the expression for m_{A}^2:

$$m_{\text{A}}^2 = \frac{B_x^2}{4\pi}\frac{1}{\tilde{r}} = \frac{B_x^2}{4\pi}\frac{2}{r_1 + r_2} = \frac{B_x^2}{4\pi}\frac{2\,(1/r_1)(1/r_2)}{1/r_1 + 1/r_2} = \frac{2\,m_{\text{on}}^2\,m_{\text{off}}^2}{m_{\text{on}}^2 + m_{\text{off}}^2} .$$

Multiplying and dividing the expression for $m_{\perp}$ by B_x^2, we finally obtain

$$m_{\perp}^2 = \frac{B_x^2}{4\pi\tilde{r}}\left(\frac{\tilde{B}_y}{B_x}\right)^2 .$$

The right-hand side of this equation contains m_{A} and tangents of the magnetic field inclination angles:

$$m_{\perp}^2 = \frac{m_{\text{A}}^2}{4}(\tan\theta_2 + \tan\theta_1)^2 . \tag{23}$$

Therefore, unlike m_{off}, m_{A}, and m_{on}, the parameter $m_{\perp}$ depends not only on the density ratio at the discontinuity but also on the magnetic field configuration.

In Section 3.3, we show that $m_{\perp}$ is the minimum plasma flux at which the transition to the perpendicular shock is possible.

2.3 Classification of discontinuities by matter flux

Formula (18) demonstrates that the mass flux m through the discontinuity surface, more precisely, its square m^2, is a suitable parameter to identify different MHD flow types. (In addition, the mass flux is proportional to the magnetic reconnection rate, which is important, for example, in astrophysical applications.) It is nonnegative. Its values (under other equal conditions and in the presence of a density jump at the discontinuity) are split into several intervals according to inequalities (21). A specific magnetic field configuration is realized inside each interval.

Using the argument given above and formula (18), we consider the function $\theta_2 = \arctan(a\tan\theta_1)$ at different admissible values of the coefficient

$$a = \frac{m^2/m_{\text{off}}^2 - 1}{m^2/m_{\text{on}}^2 - 1} ,$$

which shows how the tangential component of the magnetic field changes across the discontinuity [9]. We use the fact that inequalities (21) hold if there is a density jump at the discontinuity. We consider the behavior of the function at zero, at the points m_{off}, m_{A}, and m_{on}, and inside the mass flux intervals between these points.

As follows from (18), $a = 1$ at $m = 0$. The magnetic field inclination angle is conserved ($\theta_1 = \theta_2$). Accordingly, the tangential magnetic field component is conserved: $\{B_y\} = 0$. It follows from system (11) that there are no jumps $\{v_x\}$, $\{v_y\}$, or $\{p\}$ at the discontinuity. However, the temperature and density of the plasma can change across the discontinuity. This is a two-dimensional variant of the contact discontinuity considered in Section 2.1 (Fig. 3c).

Inside the interval $0 < m < m_{\text{off}}$, the inequalities $0 < a < 1$ hold. Therefore, $0 < \theta_2 < \theta_1$. This means that the magnetic field strength decreases across the discontinuity. The magnetic field behaves in such a way on a slow shock (Fig. 4a).

Substituting $m = m_{\text{off}}$ in (18) yields $a = 0$. The tangential magnetic field component vanishes across the discontinuity, which must be the case at the switch-off shock (Fig. 4b).

Inside the interval $m_{\text{off}} < m < m_{\text{A}}$, the inequalities $-1 < a < 0$ hold. The slow shock changes the tangential magnetic field direction, as shown in Fig. 4c.

At $m = m_{\text{A}}$, the coefficient $a = -1$. To see this, it is necessary to substitute formula (22) in the formula for a. The tangential component of the magnetic field is reversed, with its absolute values remaining unaltered. The same magnetic field configuration can be realized in the particular case of a flat Alfvén shock if $\{\rho\} = 0$. This wave is schematically shown in Fig. 3d in Section 2.1.

Substituting any value of m from the interval $m_{\text{A}} < m < m_{\text{on}}$ yields $a < -1$. The absolute value of the field strength increases, but its tangential component changes sign. Such is the behavior of a trans-Alfvénic shock (Fig. 4d).

At $m = m_{\text{on}}$, $a \to \pm\infty$. In other words, the tangential field component can arise behind the discontinuity even it was absent before it. This is a switch-on shock (Fig. 4e).

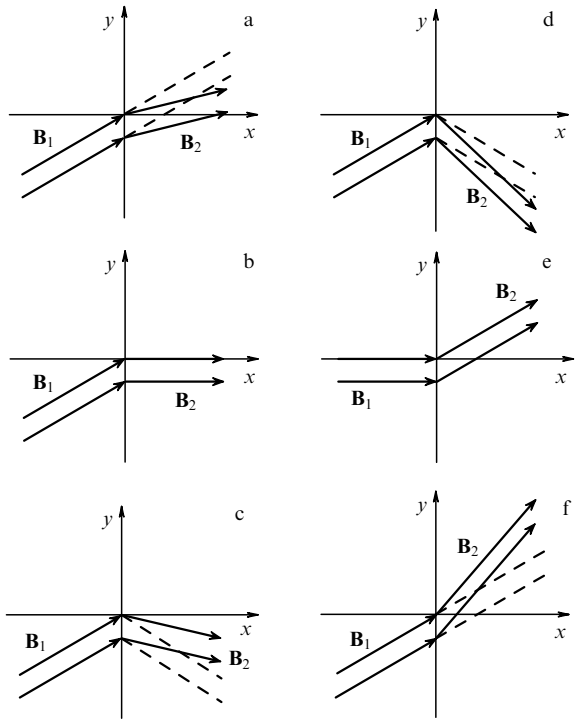

Figure 4. Oblique MHD-shocks: (a) slow shock, (b) switch-off shock, (c) slow shock reversing the tangential magnetic field, (d) trans-Alfvén shock, (e) switch-on shock, (f) fast shock.

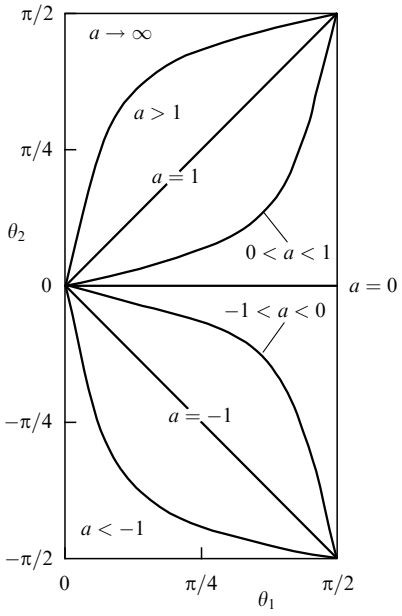

Figure 5. Possible relations between angles θ_1 and θ_2 for different types of discontinuous MHD-flows.

Finally, if $m > m_{\rm on}$, then $a > 1$. Therefore, $\theta_2 > \theta_1 > 0$. The magnetic field strength increases across the discontinuity, as must be the case for a fast shock (Fig. 4f).

Different regimes of the magnetic field behavior are shown in Fig. 5 as the plots of the function $\theta_2 = \arctan(a \tan\theta_1)$ for angles from the interval $\theta_1 \in [0; \pi/2]$. The case $\theta_1 \in [-\pi/2; 0]$ can be obtained by rotating the coordinate frame about the x axis through the angle π.

We now consider the limit values of the angle θ_1.

(1) The magnetic field is perpendicular to the discontinuity surface, i.e., $\theta_1 \to 0$. The angle θ_2 can take any value from $[0; \pi/2)$. The angle θ_2 can be zero in any regime if $\theta_1 \to 0$. A parallel shock is then formed, which is a hydrodynamic shock (Fig. 1b) propagating along the magnetic field lines. The values $\theta_2 \in (0; \pi/2)$ correspond to a switch-on shock at given values of ρ_1 and ρ_2.

(2) The magnetic field is parallel to the discontinuity surface, i.e., $\theta_1 \to \pi/2$. The angle θ_2 takes the values $\theta_2 = \pm\pi/2$. The magnetic field strength vectors are parallel to the discontinuity plane and, moreover, take the same values on different sides of the discontinuity. These properties are characteristic of two-dimensional tangential discontinuities and perpendicular shocks.

The question can arise: if the discontinuity classification is so conventional, being dependent on geometrical relations between the magnetic field line inclination angles, could the type of the observed discontinuous flow change in passing from one reference frame to another? Let the primed reference frame move relative to the laboratory (unprimed) frame with a constant velocity $\mathbf{u}$ along the discontinuity plane, such that the axes of both frames are parallel to each other. We let the magnetic field components parallel and perpendicular to the relative velocity $\mathbf{u}$ be denoted by $B_\parallel$ and $B_\perp$. Then the Lorentz transformations for the magnetic field can be written as

$$\mathbf{B}_\parallel = \mathbf{B}'_\parallel\,,$$

$$\mathbf{B}_\perp = \left(\mathbf{B}'_\perp + \frac{1}{c}\,[\mathbf{u}\times\mathbf{E}']\right)\left(1 - \frac{u^2}{c^2}\right)^{-1/2}.$$

Let the moving (primed) frame be the de Hoffmann–Teller system in which $\mathbf{E}' = 0$. Then the ratio of the parallel to the perpendicular field components gives the angle transformation in the moving (primed) to the laboratory (unprimed) reference frames in the form

$$\tan\theta' = \tan\theta\sqrt{1 - \frac{u^2}{c^2}}\,.$$

The angle transformation has the same form on each side of the discontinuity surface and therefore cannot change the qualitative relation between the angles θ_1 and θ_2. Equal angles remain equal, the larger angle remains larger. Moreover, in the nonrelativistic limit, the angles are simply preserved.

To compare two systems moving relative to each other with some velocity at which the electric field is not equal to zero, it is sufficient to pass from both systems to the de Hoffmann–Teller one and then compare the results:

$$\tan\theta'\sqrt{1 - \frac{(\mathbf{u}_{\rm HT} - \mathbf{u})^2}{c^2}} = \tan\theta\sqrt{1 - \frac{u_{\rm HT}^2}{c^2}}\,.$$

Here, u and $u_{\rm HT}$ are the velocities of the new frame and the de Hoffmann-Teller frame relative to the 'laboratory' frame. Again, we arrive at the same conclusion that the qualitative relations between the angles θ_1 and θ_2 do not change. Hence, the graphic representation of the admissible relations between the angles on the discontinuity surface obtained above (see Fig. 5) can be applied directly in the 'laboratory' reference frame. We use this property in Section 3 when considering the magnetic reconnection problem.

3. Continuous transitions between magnetohydrodynamic discontinuities

3.1 Conditions for the transitions

In Section 1, we found that each type of two-dimensional discontinuous flow corresponds to a certain region on the mass flux axis m, more precisely, m^2. Therefore, continuous transitions are possible only between discontinuities located immediately close to each other on this axis. Otherwise, the transition would require matter flux jumps. The form of the dependence $\theta_2(m^2, \theta_1)$ can be conveniently determined by two parameters, $m_{\rm off}$ and $m_{\rm on}$, although this can be done by other means, for example, by specifying the densities ρ_1 and ρ_2. To find the magnetic field from the distribution of angles, in addition, the value of B_x should be known.

We are interested in signatures of discontinuous flows, i.e., in qualitative changes between the angles θ_1 and θ_2 with varying m^2. Therefore, we temporarily consider formula (18) without specific applications to physical conditions in the plasma. We choose the values of the parameters in Eqn (18) based on requirements of clarity and simplicity. The values of $m_{\rm A}$ and $m_\perp$ are determined from Eqns (22) and (23). Let the values of ρ_1 and ρ_2 be related as 1:2. The precise values of $m^2_{\rm off}, m^2_{\rm A}$, and $m^2_{\rm on}$ are then related as 3:4:6. With this in mind, the mass flux square is measured in units of $m^2_{\rm A}/4$.

Figure 6 shows the plots of $\theta_2(m^2)$ for three values of the magnetic field inclination angle before the discontinuity: $\theta_1 = 5^\circ$, 25°, and 45° [71]. We see that the curves $\theta_2(m^2)$ demonstrate similar behavior. First, they all cross at one point at $m^2 = m^2_{\rm off} = 3$. Second, for each curve, $\theta_2 \to -\theta_1$ as $m^2 \to m^2_{\rm A} = 4$. Third, in all plots, there is a region that does not satisfy conditions (19) and (20). This region lies in the vicinity of the point $m^2 = m^2_{\rm on} = 6$.

We identify four regions in Fig. 6 with the characteristic behavior of the function $\theta_2(m^2)$. In region I ($0 < m^2 < 3$), the component B_{y2} of the magnetic field $\mathbf{B}_2$ decreases with increasing m^2. Here, $0 < \theta_2 < \theta_1$, i.e., the tangential magnetic field component decreases across the discontinuity surface. At $m^2 = 3$, the tangential component B_{y2} vanishes across the discontinuity. In region II ($3 < m^2 < 4$), the component B_{y2} is negative and increases by the absolute value, but now $-\theta_1 < \theta_2 < 0$. In region III ($4 < m^2 < 6$), as in region II, the tangential component B_y changes sign across the discontinuity. However, in this case, the absolute value of B_y increases ($\theta_2 < -\theta_1$). Finally, in region IV ($m^2 > 6$), the magnetic field increases ($\theta_2 > \theta_1$), preserving its sign.

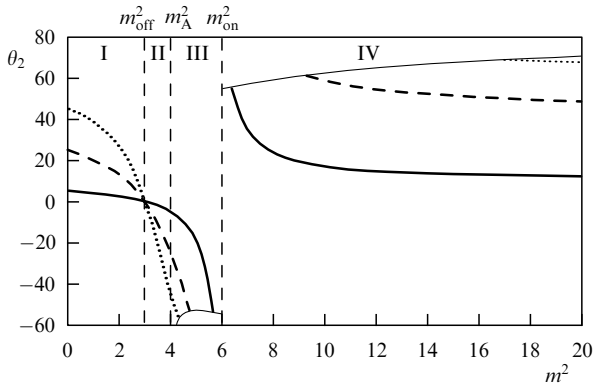

Figure 6. The magnetic field inclination angle θ_2 behind the discontinuity plane as a function of the mass flux squared m^2 for different angles θ_1. The solid, dashed, and dotted lines show the respective cases $\theta_1 = 5^\circ$, 25°, and 45°. All plots $\theta_2(m^2)$ for different θ_1 end at the curve shown by the thin line.

At the boundary between regions II and III, $m^2 = m^2_{\rm A}$. The domain of the function $\theta_2(m^2, \theta_1)$ to the left and to the right of $m^2_{\rm A}$ is defined by respective conditions (19) and (20). As $m^2 \to m^2_{\rm A}$, $\tilde{B}^2_y \to 0$, and condition (20) becomes $m^2 > m^2_{\rm A}$. Therefore, the function $\theta_2(m^2, \theta_1)$ is defined near $m^2_{\rm A}$ in both regions II and III (see Fig. 6). However, with increasing m^2, the right-hand side of inequality (20) increases as well. At some value of m^2 in region III, these values becomes equal to each other. A maximum strong trans-Alfvénic shock (at the maximum increase in the magnetic field energy) emerges. With a further increase in the mass flux, the value of m^2 cannot satisfy conditions (19) and (20) until m^2 again becomes comparable to $m^2_{\rm A} + m^2_\perp$. This happens in region IV, where the strongest fast shock is observed.

We derive an equation for the curve on which the free ends of the plots lie and hence, for a given relation between the plasma density ρ_1 and ρ_2, the strongest fast and trans-Alfvénic shocks occur. We equate m^2 to the right-hand side of (14):

$$m^2 = \frac{B_x^2 + \tilde{B}_y^2}{4\pi\tilde{r}}\,.$$

Hence,

$$B_{y1} = \pm 2\sqrt{4\pi\tilde{r}m^2 - B_x^2} - B_{y2}\,,$$

where the signs $-$ and $+$ correspond to respective regions III ($m_{\rm A} < m < m_{\rm on}$) and IV ($m > m_{\rm on}$). We divide the obtained equation by B_x. Then

$$\tan\theta_1 = \pm 2\sqrt{\frac{m^2}{m^2_{\rm A}} - 1} - \tan\theta_2\,. \tag{24}$$

After substituting Eqn (24) in (18), we obtain an equation for the sought curve:

$$\tan\theta_2 = \pm 2\,\frac{m^2/m^2_{\rm off} - 1}{m^2/m^2_{\rm off} + m^2/m^2_{\rm on} - 2}\sqrt{\frac{m^2}{m^2_{\rm A}} - 1}\,.$$

We simplify this equation by using relation (22):

$$\tan\theta_2 = \pm\frac{m^2/m^2_{\rm off} - 1}{\sqrt{m^2/m^2_{\rm A} - 1}}\,. \tag{25}$$

In Fig. 6, the thin line shows the plot of curve (25).

With a further increase in the mass flux, the tangent of the magnetic field inclination angle behind the discontinuity tends asymptotically from above to the value

$$\tan\theta_2 = \frac{m^2_{\rm on}}{m^2_{\rm off}}\tan\theta_1\,,$$

or, after expanding $m_{\rm off}$ and $m_{\rm on}$,

$$\tan\theta_2 = \frac{\rho_2}{\rho_1}\tan\theta_1\,. \tag{26}$$

Multiplying equation (26) by B_x, we obtain

$$B_{y2} = \frac{\rho_2}{\rho_1}\,B_{y1}\,. \tag{27}$$

Such a form of the dependence between the magnetic field strength on different sides of the discontinuity surface is typical for perpendicular shocks. This is related to the possibility of a continuous transition between shocks, which is considered in Section 3.3. In the next subsection, we start studying the transitions occurring when the mass flux changes.

3.2 Transitions with matter flux changes

Figure 6 demonstrates how the character of the relation between the magnetic field inclination angles and, hence, the type of discontinuous MHD flow, changes with gradually increasing the plasma flow. At $m^2 = 0$, a contact discontinuity (C) arises. Regions I and II correspond to slow MHD shocks that do not reverse ($S_-^{\uparrow}$) and do reverse ($S_-^{\downarrow}$) the magnetic field tangential component. They are separated by the switch-off shock (S_{off}). At the boundary between regions II and III, conditions for the formation of an Alfvén discontinuity (A) hold. Trans-Alfvénic shocks (Tr) are in region III, and fast shocks (S_+) are in region IV. A switch-on shock (S_{on}) can form at the boundary between regions III and IV.

In any of these variants, the transition solutions for discontinuous flows corresponding to neighboring regions are realized for the mass flux square separating these two regions on the coordinate plane (see Fig. 6). We consider all adjacent pairs of discontinuities of different types one by one and search for the transition solution for each pair. We start with a zero mass flux and then increase its value.

At a zero mass flux, a contact discontinuity is formed. Region I, occupied by slow shocks, joins it. Therefore, in the entire set of two-dimensional discontinuous flows, the transition from a contact discontinuity to a slow shock is only possible with a continuous change in the mass flux. We verify this.

The full system of boundary conditions at the slow shock coincides with the general equations for oblique shocks, which follow from the full system of equations (1)–(8) with $v_z = 0$ and $B_z = 0$:

$$
\begin{aligned}
&B_z = 0\,, \quad v_z = 0\,,\\
&\{B_x\} = 0\,, \quad \{\rho v_x\} = 0\,,\\
&\left\{ p + \rho v_x^2 + \frac{B^2}{8\pi} \right\} = 0\,,\\
&\left\{ \rho v_x \left(\frac{v^2}{2} + \epsilon + \frac{p}{\rho} \right) + \frac{B_y}{4\pi} (v_x B_y - v_y B_x) \right\} = 0\,,\\
&\{v_x B_y - v_y B_x\} = 0\,, \quad \left\{ \rho v_x v_y - \frac{1}{4\pi} B_x B_y \right\} = 0\,.
\end{aligned}
\tag{28}
$$

The solution of these equations in region I shown in Fig. 6 indeed corresponds to a slow shock ($S_-^{\uparrow}$), which does not reverse the sign of the magnetic field tangential component. This can be easily verified at small m^2. For example, formula (18), which is applicable to two-dimensional discontinuous flows like (28), implies that

$$
\tan\theta_2 \approx \left(1 - \frac{m^2}{m_{off}^2} + \frac{m^2}{m_{on}^2} \right) \tan\theta_1\,,
$$

and hence, due to inequalities (21), $0 < \theta_2 < \theta_1$, as must be the case in a slow shock. Moreover, as $m^2 \to 0$, i.e., $v_x \to 0$, we have $\theta_2 \to \theta_1$, which is the natural limit case for slow shocks.

We show that at $m = 0$, i.e., when $v_x = 0$, boundary conditions (28) also satisfy the contact discontinuity conditions. Indeed, substituting $v_x = 0$ in system of equations (28) yields

$$
\begin{aligned}
&B_z = 0\,, \quad v_z = 0\,, \quad v_x = 0\,,\\
&\{B_x\} = 0\,, \quad \{v_y\} = 0\,,\\
&\{B_y\} = 0\,, \quad \{p\} = 0\,.
\end{aligned}
\tag{29}
$$

Boundary conditions (29) immediately imply that the magnetic field strength is continuous, i.e., $\mathbf{B}_1 = \mathbf{B}_2$, and the density jump $\{\rho\}$ is nonzero, as must be the case at a contact discontinuity. Thus, system of equations (29) describes both slow shocks in the limit $v_x \to 0$ and contact discontinuities, i.e., is a transition solution.

We return to Fig. 6. Region II, like region I, corresponds to slow shocks; however, in region II, the tangential magnetic field component changes sign across the discontinuity surface. At the boundary between these two regions, $m = m_{off}$. At this value of the mass flux, according to formula (18), the magnetic field is perpendicular to the discontinuity plane. With other conditions being equal, this is true for any initial angle θ_1 that corresponds to the intersection of the curves in Fig. 6. These properties define a switch-off shock. Therefore, the transition between the slow shock that does not reverse the tangential magnetic field (region I in Fig. 6) and the shock that reverses the tangential field component (region II in Fig. 6) occurs via a switch-off shock. To find the boundary conditions for this transition, we substitute the condition $B_{y2} = 0$ obtained from (18) with $m = m_{off}$ in the system of equations for oblique waves (28) to obtain

$$
\begin{aligned}
&B_z = 0\,, \quad v_z = 0\,, \quad B_{y2} = 0\,,\\
&\{B_x\} = 0\,, \quad \{\rho v_x\} = 0\,,\\
&\{p + \rho v_x^2\} = \frac{B_{y1}^2}{8\pi}\,,\\
&\left\{ \frac{v^2}{2} + \epsilon + \frac{p}{\rho} \right\} = \{v_y\} v_{y2}\,,\\
&B_x\{v_y\} = -v_{x1} B_{y1}\,, \quad \rho v_x \{v_y\} = -\frac{1}{4\pi} B_x B_{y1}\,.
\end{aligned}
\tag{30}
$$

The next transition solution is sought at the right boundary of region II for $m = m_A$. The corresponding transition occurs between the slow shock reversing the tangential magnetic field ($S_-^{\downarrow}$) and a flow whose type is to be established. Equation (12) with $m = m_A$ can be satisfied only if $\{r\} = 0$, i.e., $\{\rho\} = 0$. Substituting the last condition in (28) yields

$$
\begin{aligned}
&B_z = 0\,, \quad v_z = 0\,,\\
&\{\rho\} = 0\,, \quad \{B_x\} = 0\,, \quad \{v_x\} = 0\,,\\
&\left\{ p + \frac{B^2}{8\pi} \right\} = 0\,, \quad \{\epsilon\} = 0\,,\\
&B_x\{v_y\} = v_x\{B_y\}\,, \quad \rho v_x \{v_y\} = \frac{1}{4\pi} B_x \{B_y\}\,.
\end{aligned}
\tag{31}
$$

In the case $\{B_y\} = 0$, all quantities are continuous, and there is no discontinuity. Therefore, we consider the case $\{B_y\} \neq 0$. We substitute m_A in Eqn (18). Using expression (22), we find that $B_{y2} = -B_{y1}$. Then solution (31) describes a particular two-dimensional case of the Alfvén discontinuity. To see this, we substitute $\{\rho\} = 0$ in system of equations (1)–(8). As a

result, we find the boundary conditions for the Alfvén discontinuous flow:

$$\begin{aligned}
&\{\rho\} = 0\,, \quad \{B_x\} = 0\,, \quad \{v_x\} = 0\,,\\
&\left\{p + \frac{B^2}{8\pi}\right\} = 0\,, \quad \{\epsilon\} = 0\,,\\
&B_x\{v_y\} = v_x\{B_y\}\,, \quad \rho v_x\{v_y\} = \frac{1}{4\pi}\,B_x\{B_y\}\,,\\
&B_x\{v_z\} = v_x\{B_z\}\,, \quad \rho v_x\{v_z\} = \frac{1}{4\pi}\,B_x\{B_z\}\,.
\end{aligned} \tag{32}$$

A comparison of (31) and (32) shows that boundary conditions (31) describe a two-dimensional Alfvén discontinuity such that the velocity and magnetic field vectors lie in the (x, y) plane. Therefore, system (31) represents a transition solution between the slow shock reversing the tangential magnetic field component in the limit $\{\rho\} \to 0$ and the Alfvén discontinuous flow at $v_z = 0$, $B_z = 0$.

Eliminating the ratio $\{B_y\}/\{v_y\}$ from the last two equations of system (31), we obtain the mass flux squared corresponding to the Alfvén velocity $m^2 = \rho B_x^2/4\pi$. We stress that ρ in this expression is the plasma density at the Alfvén discontinuity at which the transition from the two-dimensional discontinuous flow occurs. There is no density jump at the Alfvén discontinuity, and the density ρ, generally speaking, does not coincide with ρ_1 or ρ_2 that appeared in considering two-dimensional discontinuous flows. This density can be found from comparing the Alfvén mass flux and the value that was previously denoted by m_A [see inequalities (13) and (19)]: $\rho = 1/\tilde{r}$.

Region III joins the value $m = m_A$ from the right in Fig. 6. In this region lie trans-Alfvénic discontinuities, which reverse and increase the magnetic field tangential component. The trans-Alfvénic discontinuous flow (Tr) satisfies inequality (14). When the mass flux square tends to $m^2 = (B_x^2 + \tilde{B}_y^2)/4\pi\tilde{r}$, the jump $\{B_y\}$ vanishes. Thus, a smooth transition of the mass flux to m_A occurs. The transition conditions between the trans-Alfvénic shocks and the Alfvén discontinuity are nearly identical to those in the preceding case of the transition from slow shocks, the difference being that the transition from slow and trans-Alfvénic shocks occurs at the respective maximum and minimum possible mass flux. The transition solution is described by system of equations (31).

Inside some mass flux interval near the boundary between regions II and IV, no discontinuous flow can be realized, which makes it impossible to continuously change the mass flux from the region of trans-Alfvénic shocks to the region of fast shocks. This interval decreases as the initial magnetic field inclination angle decreases, until its vanishing at $\theta_1 = 0$ (see Fig. 6). The possible mass fluxes of fast shocks are restricted by the same inequality (14) as the trans-Alfvénic shocks. The fastest shock (that maximally increases the magnetic field energy) is realized at the minimum possible mass flux squared, $m^2 = (B_x^2 + \tilde{B}_y^2)/4\pi\tilde{r}$. But now, unlike in the trans-Alfvénic case, the jump $\{B_y\}$ does not tend to zero; it is finite and can be found from the solution of Eqn (17). This explains the different possible mass fluxes for trans-Alfvénic and fast shocks.

3.3 Transitions at zero flow parameters

As was shown in Section 2.3, some discontinuous flows occur at the limit flow parameters. Variations of ρ_1, $\{\rho\}$, and B_x squeeze or stretch the plots shown in Fig. 6 along the coordinate axes while preserving their general structure. For zero values of θ_1, B_x, and $\{\rho\}$, the behavior of $\theta_2(m^2)$ is schematically shown in Fig. 7.

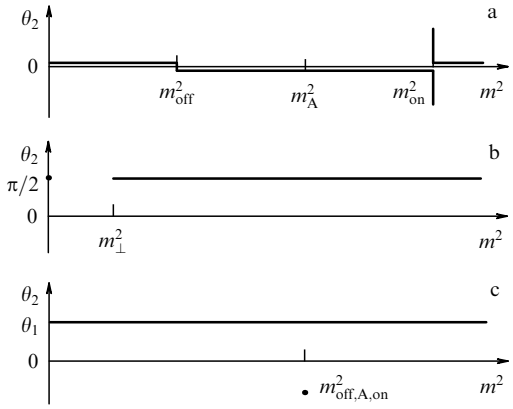

Figure 7. Schematic behavior of $\theta_2(m^2)$ for $\theta_1 = 0$ (a), $B_x = 0$ (b), and $\{\rho\} = 0$ (c).

Decreasing the angle θ_1 also decreases the gap between the allowed mass flux for the fast and trans-Alfvénic shocks (see Fig. 6). Under the conditions in Fig. 7a, a transition between them can occur at $\theta_1 = 0$. Boundary conditions (28) here take the form

$$\begin{aligned}
&B_z = 0\,, \quad v_z = 0\,, \quad B_{y1} = 0\,,\\
&\{B_x\} = 0\,, \quad \{\rho v_x\} = 0\,,\\
&\{p + \rho v_x^2\} = -\frac{B_{y2}^2}{8\pi}\,,\\
&\left\{\frac{v^2}{2} + \epsilon + \frac{p}{\rho}\right\} = \{v_y\}v_{y2}\,,\\
&B_x\{v_y\} = v_{x2}B_{y2}\,, \quad \rho v_x\{v_y\} = \frac{1}{4\pi}\,B_xB_{y2}\,.
\end{aligned} \tag{33}$$

From the common solution of the last two equations of system (33), we have

$$m^2 = \frac{\rho_2 B_x^2}{4\pi} = m_{on}^2\,.$$

Thus, a continuous transition indeed occurs at the boundary between regions II and IV, where trans-Alfvénic and fast shocks are located. For $m = m_{on}$, Eqn (18) cannot be solved uniquely. The zero value of θ_1 can correspond to a nonzero value of θ_2. Behind the shock front, a tangential magnetic field appears. Such a shock is called a switch-on shock (S_{on}). It can play the role of a transition solution for the trans-Alfvénic and fast shocks in the limit $\theta_1 \to 0$, but for the transition to occur, the mass flux must tend to m_{on}.

For any other values $m \neq m_{on}$, Eqn (18) implies that when the angle θ_1 vanishes, the angle θ_2 also vanishes. In other words, if $B_{y1} = 0$, then $B_{y2} = 0$ (Fig. 7a). Here, the boundary conditions for two-dimensional discontinuous flows (28) are written in the form

$$\begin{aligned}
&B_z = 0\,, \quad v_z = 0\,, \quad B_y = 0\,,\\
&\{B_x\} = 0\,, \quad \{\rho v_x\} = 0\,,\\
&\{p + \rho v_x^2\} = 0\,, \quad \left\{\frac{v^2}{2} + \epsilon + \frac{p}{\rho}\right\} = 0\,, \quad \{v_y\} = 0\,.
\end{aligned} \tag{34}$$

System of equations (34) includes boundary conditions of the ordinary hydrodynamic shock. However, due to the conditions $B_{y1} = 0$ and $B_{y2} = 0$, such a shock propagates along the magnetic field lines. This is a parallel shock ($S_{\parallel}$). System of equations (34) represents a transition solution between oblique shocks in the limit $\theta_1 \to 0$ and a parallel shock.

To find the form of the transition solution between a parallel shock and a contact discontinuity, we set $v_x = 0$ in (34):

$$\begin{aligned} &B_z = 0\,, \quad v_z = 0\,, \quad B_{y1} = 0\,, \\ &\{B_x\} = 0\,, \qquad \{p\} = 0\,, \qquad \{v_y\} = 0\,. \end{aligned} \tag{35}$$

This system of equations corresponds to contact discontinuity (29), which is orthogonal to magnetic field lines. Hence, it describes the transition solution between a parallel shock in the limit as $v_x \to 0$ and a contact discontinuity.

When the magnetic flux ($B_x = 0$) vanishes, $m_{\rm on}$ separating regions III and IV in Fig. 6 formally vanishes. Thus, all nonzero mass fluxes prove to be in region IV (Fig. 7b). Therefore, the transition in this case is from a fast shock. To determine the type of discontinuous flow in this case, we find the boundary conditions for the transition solution by substituting $B_x = 0$ in (28):

$$\begin{aligned} &B_z = 0\,, \qquad v_z = 0\,, \qquad B_x = 0\,, \\ &\{\rho v_x\} = 0\,, \qquad \left\{p + \rho v_x^2 + \frac{B^2}{8\pi}\right\} = 0\,, \\ &\left\{\rho v_x\left(\frac{v^2}{2} + \epsilon + \frac{p}{\rho}\right) + v_x\,\frac{B^2}{4\pi}\right\} = 0\,, \\ &\{v_x B_y\} = 0\,, \qquad \{v_y\} = 0\,. \end{aligned} \tag{36}$$

These conditions represent a compression shock propagating orthogonally to the magnetic field, i.e., a perpendicular shock ($S_{\perp}$). The magnetic field lines are parallel to the y axis. Of course, in the general case, the magnetic field direction can be different from the direction of the coordinate system axes. After substituting $B_x = 0$ in Eqns (1)–(8), we find the boundary conditions for the orthogonal shock:

$$\begin{aligned} &B_x = 0\,, \\ &\{\rho v_x\} = 0\,, \qquad \left\{p + \rho v_x^2 + \frac{B^2}{8\pi}\right\} = 0\,, \\ &\left\{\rho v_x\left(\frac{v^2}{2} + \epsilon + \frac{p}{\rho}\right) + v_x\,\frac{B^2}{4\pi}\right\} = 0\,, \\ &\{v_x B_y\} = 0\,, \qquad \{v_y\} = 0\,, \\ &\{v_x B_z\} = 0\,, \qquad \{v_z\} = 0\,. \end{aligned} \tag{37}$$

The equations in system (36) represent boundary conditions for a transition discontinuity between a fast shock in the limit $B_x \to 0$ and a perpendicular shock with the magnetic field parallel to the y axis. We note that this transition can occur only for the mass fluxes satisfying inequality (20), which at $B_x = 0$ takes the form $m^2 > m_{\perp}^2$. Relation (27), derived in Section 3.1 for fast shocks in the limit of large mass fluxes, is also valid for Eqns (36) and (37).

We now determine the boundary conditions for the discontinuity that arises at $m^2 = 0$ in Fig. 7b. For this, we substitute $B_x = 0$ and $v_x = 0$ in system of equations (1)–(8). In this case, the magnetic field and velocity are parallel to the discontinuity surface and their absolute values and directions can have arbitrary jumps:

$$\begin{aligned} &B_x = 0\,, \qquad v_x = 0\,, \\ &\left\{p + \frac{B^2}{8\pi}\right\} = 0\,. \end{aligned} \tag{38}$$

This is a tangential discontinuity (T). In the limit $B_x \to 0$, both a contact discontinuity and a slow shock, as well as an Alfvén discontinuity, can pass into it. We obtain the corresponding transition solutions.

Substituting $B_x = 0$ in the boundary conditions for contact discontinuity (29) yields the following transition solution:

$$\begin{aligned} &B_z = 0\,, \qquad v_z = 0\,, \qquad B_x = 0\,, \qquad v_x = 0\,, \\ &\{B_y\} = 0\,, \qquad \{v_y\} = 0\,, \qquad \{p\} = 0\,. \end{aligned} \tag{39}$$

System of equations (39) describes tangential discontinuity (38) for the zero field component B_z in the absence of jumps $\{v_y\}$ and $\{B_y\}$.

The boundary conditions of oblique shocks (28) for $B_x = 0$ and $v_x = 0$ are transformed to the form

$$\begin{aligned} &B_z = 0\,, \qquad v_z = 0\,, \qquad B_x = 0\,, \qquad v_x = 0\,, \\ &\left\{p + \frac{B^2}{8\pi}\right\} = 0\,. \end{aligned} \tag{40}$$

Transition solution (40) corresponds to the flat tangential discontinuity (38) at $B_z = 0$.

The transition solution from the Alfvén discontinuity can be found by substituting $B_x = 0$ in system (32):

$$\begin{aligned} &B_x = 0\,, \\ &\{\rho\} = 0\,, \qquad \left\{p + \frac{B^2}{8\pi}\right\} = 0\,. \end{aligned} \tag{41}$$

Boundary conditions (41) describe tangential discontinuity (38) without a density jump.

When the magnetic flux through the discontinuity decreases, the trans-Alfvénic shocks occupying region III in Fig. 6 degenerate into a particular case of the Alfvén discontinuity. This can be observed in Fig. 6 as a gradual decrease in the mass flux intervals inside which the trans-Alfvénic discontinuities can appear as the magnetic field incidence angle θ_1 increases.

Of course, for any type of flow, the density jump can be set to zero. In this case, all parameters $m_{\rm off}^2$, $m_{\rm A}^2$, and $m_{\rm on}^2$ are equal to flux (22) at which Alfvén discontinuity (34) is formed. The point $m_{\rm off,\,A,\,on}^2$ in Fig. 7c corresponds to this discontinuity. For different values of the mass flux, a difference in the plasma characteristics on each side of the discontinuity surface disappears. The discontinuity plane then corresponds to an arbitrary plane in the homogeneous medium. The discontinuity as such is then absent.

3.4 Scheme of continuous transitions

The obtained transition solutions allow visualizing the pattern of possible continuous transitions between discontinuous MHD flows [9]. The first scheme of transitions, based on the transition solutions known at that time, was proposed by Syrovatskii [7]. It included transitions between discontinuous flows of only four types: tangential discontinuities (T) and

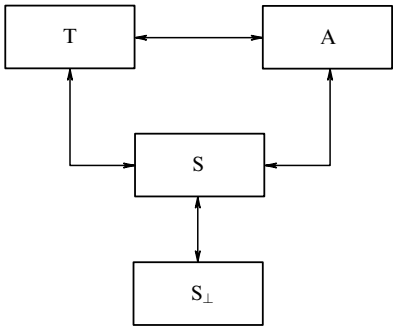

Figure 8. Schematic of continuous transitions among MHD discontinuities [7].

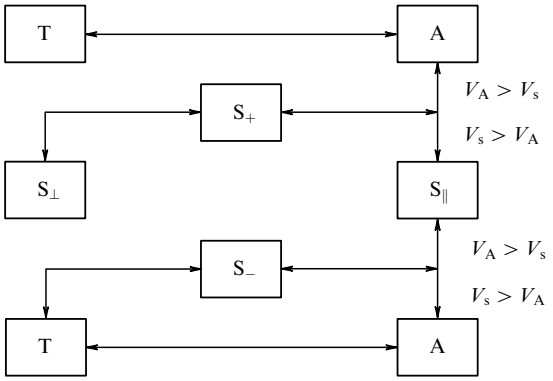

Figure 9. Schematic of continuous transitions among MHD discontinuities [72].

Alfvén (A), oblique (S), and perpendicular ($S_\perp$) shocks (Fig. 8).

Clearly, this scheme is not complete. First, it does not include some discontinuous MHD solutions, in particular, parallel shocks ($S_\parallel$) and contact discontinuities (C). Second, the notion of an 'oblique shock' (S) includes many different types of discontinuous flows: fast (S_+) and slow (S_-) shocks, switch-on (S_{on}) and switch-off (S_{off}) shocks, and trans-Alfvénic shocks (Tr).

Later, the picture of transitions between discontinuous flows was completed [72] using the correspondence between shocks and low-amplitude waves in MHD [8]. The scheme of transitions based on the diagram of low-amplitude wave phase velocities is presented in Fig. 9. Although this approach correctly predicts possible continuous transitions between discontinuous flows and even the conditions for such transitions, it does not describe the specific form of the transition solutions between the considered discontinuities. Also, this scheme still lacks many types of discontinuities.

The results obtained in Sections 3.1 and 3.2 enable us to construct the general scheme of possible continuous transitions between discontinuous MHD flows (Fig. 10). Three-dimensional discontinuous flows are in the upper row of the scheme. Two-dimensional discontinuous flows are in the middle row of the scheme in the order of increasing mass flux through the discontinuity surface. One-dimensional parallel shocks ($S_\parallel$) are in the bottom row. The individual elements are grouped in order to conveniently compare our scheme of transitions with earlier ones.

Syrovatskii's scheme shown in Fig. 8 [7] is in agreement with the scheme shown in Fig. 10 if the elements $S_-^\downarrow$, S_{off}, $S_-^\uparrow$, Tr, S_{on}, and S_+ are joined into one 'oblique wave' block (S), the possible transitions inside the block are ignored, and the contact discontinuities (C) and parallel shocks (S) are omitted.

The scheme shown in Fig. 9, proposed by Somov [8] (see also [69, 72]), includes a parallel shock ($S_\parallel$) and divides oblique shocks into a block of 'slow' discontinuous flows (S_-) corresponding to condition (13) and a block of 'fast' (S_+) flows, corresponding to condition (14). Symbols V_A and V_s in Fig. 9 denote the Alfvén velocity and the speed of sound. These conditions for the transition are obtained from a comparison of the properties of discontinuities and low-amplitude waves. We verify these conditions for shocks.

We first consider the transition of oblique shocks to the Alfvén discontinuity. We note that the term $-\{p\}/\{r\}$ in Eqn (12) is proportional to the mass flux moving with the speed of sound. Indeed,

$$-\frac{\{p\}}{\{r\}} = \rho_1\rho_2\,\frac{\{p\}}{\{\rho\}} \propto \rho^2\,\frac{\partial p}{\partial \rho} = (\rho V_s)^2\,. \tag{42}$$

The transition of oblique shocks to the Alfvén discontinuity, according to the new generalized scheme of transitions, occurs as $m^2 \to m_A^2$; near m_A^2, we have

$$\frac{m^2 - B_x^2/4\pi\tilde{r}}{m^2 - (B_x^2 + \tilde{B}_y^2)/4\pi\tilde{r}} < 1$$

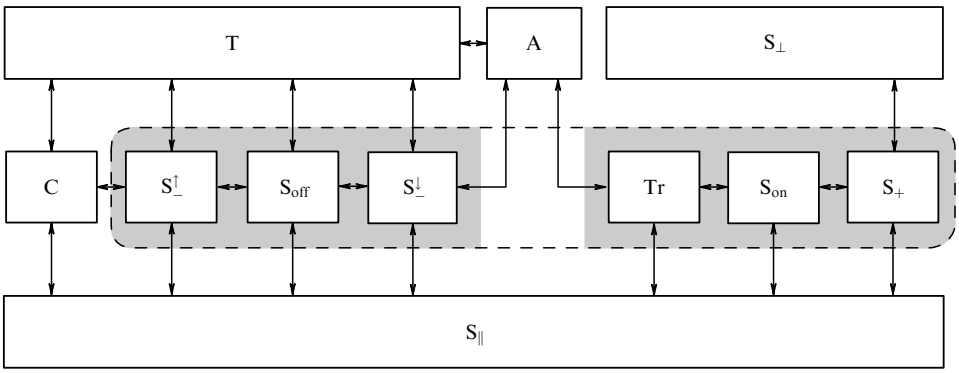

Figure 10. Generalized schematic of continuous transitions among MHD discontinuities. For comparison, the dashed-line contour shows a set of discontinuities corresponding to the oblique shock block in [7]. The gray background inside the contour shows 'slow' (on the left) and 'fast' (on the right) blocks in [72].

for (13) and

$$\frac{m^2 - B_x^2/4\pi\tilde{r}}{m^2 - (B_x^2 + \tilde{B}_y^2)/4\pi\tilde{r}} > 1$$

for (14). Using Eqns (12) and (42), we then deduce that as in Fig. 9, the transition to the Alfvén discontinuity occurs at $V_s > V_A$ for the 'slow' block (14) and at $V_A > V_s$ for the 'fast' block (13).

We now consider the transition from oblique shocks to a parallel shock. As $m^2 \to 0$ and $m^2 \to \infty$, we respectively obtain $V_s \to 0$ and $V_s \to \infty$. Thus, in transitions from oblique shocks to a parallel shock, $V_A > V_s$ for (14) and $V_s > V_A$ for (13), which had to be proved.

In Fig. 9, the transition from the parallel shock to the Alfvén discontinuity is also shown. Substituting the Alfvén discontinuity condition $\{\rho\} = 0$ in the boundary conditions of parallel shocks (34), we obtain zero jumps for all variables. Thus, the transformation of the parallel shock into an Alfvén shock is possible only when the discontinuity is eliminated and cannot be treated as a continuous transition between discontinuous flows.

We also note the impossibility of continuous transitions between slow and fast shocks and the Alfvén discontinuity, which was noted in [5]. The transition is only possible from a flat Alfvén discontinuity to a nonevolutionary trans-Alfvénic shock and a slow shock reversing the tangential magnetic field. Only after that does the transition to the fast and slow shocks via respective switch-on and switch-off shocks occur.

Combining the above considerations, we see that the proposed scheme of continuous transitions between discontinuous solutions of the ideal MHD equations is a correct generalization and extension of two earlier incomplete schemes.

We stress that the generalized scheme includes discontinuities that are nonevolutionary both in ideal MHD (trans-Alfvénic shocks) [73–75] and in dissipative MHD (for example, the Alfvén discontinuity and the switch-on shock). Modern numerical simulations often demonstrate the presence of nonevolutionary regions (ignoring their specificity). In this connection, it is necessary to accurately consider the arising conditions of such discontinuous flows, including the possibility of the transition of an evolutionary discontinuity into a nonevolutionary one under a gradual change of the flow parameters. The generalized scheme allows estimating the possibility of such transitions under different conditions in plasma with a magnetic field. Such a transition is observed, in particular, in the analytic model of magnetic reconnection [54, 55]. We return to the analysis of this model in Section 7.2. However, we first consider plasma heating in discontinuous MHD flows.

4. Plasma heating at magnetohydrodynamic discontinuities

4.1 Internal energy jump

Many phenomena in cosmic and laboratory plasmas are related to a fast change in the magnetic field configuration. These processes can be accompanied by the formation of a variety of discontinuous MHD flows of different types, which exist simultaneously and change with time. The strong magnetic field reconnection provides an important example. This process gives rise to the formation of accelerated plasma flows (jets), the acceleration of charged particles to high energies, and the heating of plasma inside and outside the reconnection region. The effect of discontinuous plasma flows in the plasma thermal energy turns out to be important.

To establish the ability of a discontinuity to heat the plasma, following [9], we consider boundary condition (8), which represents the energy conservation law. Using Eqn (2), we find the internal energy jump from (8):

$$\{\epsilon\} = -\left\{\frac{v^2}{2}\right\} - \frac{1}{m}\{v_x p\} - \frac{1}{4\pi m}\left\{B^2 v_x - (\mathbf{vB})\, B_x\right\}. \quad (43)$$

The right-hand side of (43) includes three terms. Using the mean of the velocities $\tilde{v}_x$, $\tilde{v}_y$, and $\tilde{v}_z$, we write the first term in the form

$$-\left\{\frac{v^2}{2}\right\} = -\tilde{v}_x\{v_x\} - \tilde{v}_y\{v_y\} - \tilde{v}_z\{v_z\}.$$

The jumps of the tangential velocity components can be expressed in terms of the jumps of the magnetic field tangential components using Eqns (5) and (6) subject to conditions (1) and (2). We obtain

$$\{v_y\} = \frac{B_x}{4\pi m}\{B_y\}, \qquad \{v_z\} = \frac{B_x}{4\pi m}\{B_z\}.$$

Now, the first term in the right-hand side of (43) has the form

$$-\left\{\frac{v^2}{2}\right\} = -\tilde{v}_x\{v_x\} - \frac{\tilde{v}_y B_x}{4\pi m}\{B_y\} - \frac{\tilde{v}_z B_x}{4\pi m}\{B_z\}. \quad (44)$$

In the second term in the right-hand side of (43), written as

$$-\frac{1}{m}\{v_x p\} = -\frac{\tilde{p}}{m}\{v_x\} - \frac{\tilde{v}_x}{m}\{p\},$$

we substitute the pressure jump from Eqn (7), namely,

$$\{p\} = -m\{v_x\} - \frac{\tilde{B}_y}{4\pi}\{B_y\} - \frac{\tilde{B}_z}{4\pi}\{B_z\}.$$

Here, as in (43), condition (2) was used. The second term in the right-hand side of (43) finally takes the form

$$-\frac{1}{m}\{v_x p\} = -\frac{\tilde{p}}{m}\{v_x\} + \tilde{v}_x\{v_x\} + \frac{\tilde{v}_x\tilde{B}_y}{4\pi m}\{B_y\} + \frac{\tilde{v}_x\tilde{B}_z}{4\pi m}\{B_z\}. \quad (45)$$

In the third term in the right-hand side of (43), we expand the dot product **vB**:

$$-\frac{1}{4\pi m}\left\{B^2 v_x - (\mathbf{vB})B_x\right\} = -\frac{1}{4\pi m}\left\{(v_x B_y - v_y B_x)B_y + (v_x B_z - v_z B_x)B_z\right\}.$$

To the obtained equality, we apply conditions (3) and (4):

$$-\frac{1}{4\pi m}\left\{B^2 v_x - (\mathbf{vB})B_x\right\} = -\frac{v_x B_y - v_y B_x}{4\pi m}\{B_y\} - \frac{v_x B_z - v_z B_x}{4\pi m}\{B_z\}. \quad (46)$$

Thus, each of the three terms in the right-hand side of (43) is expressed through separate jumps of the normal velocity component and the tangential magnetic field component.

After substituting (44)–(46) in (43), we obtain

$$\{\epsilon\} = -\frac{\tilde{p}}{m}\{v_x\} + \frac{\tilde{v}_x\tilde{B}_y - \tilde{v}_y B_x}{4\pi m}\{B_y\} - \frac{v_x B_y - v_y B_x}{4\pi m}\{B_y\} + \frac{\tilde{v}_x\tilde{B}_z - \tilde{v}_z B_x}{4\pi m}\{B_z\} - \frac{v_x B_z - v_z B_x}{4\pi m}\{B_z\}.$$

This equation is significantly simplified if the means of the velocity and the magnetic field are expanded:

$$\{\epsilon\} = -\frac{\tilde{p}}{m}\{v_x\} - \frac{\{v_x\}\{B_y\}}{16\pi m}\{B_y\} - \frac{\{v_x\}\{B_z\}}{16\pi m}\{B_z\}.$$

Writing $-\{v_x\}/m = -\{r\}$ as a common factor, we find the final equation expressing the internal energy jump at the discontinuity in terms of the jumps of the inverse density and tangential magnetic field components:

$$\{\epsilon\} = -\{r\}\left(\tilde{p} + \frac{\{B_y\}^2 + \{B_z\}^2}{16\pi}\right). \tag{47}$$

For two-dimensional flows, Eqn (47) takes a very simple form:

$$\{\epsilon\} = -\{r\}\left(\tilde{p} + \frac{\{B_y\}^2}{16\pi}\right). \tag{48}$$

Clearly, the heating due to the parallel shock is independent of the magnetic field, because formula (48) contains only tangential field components, which are absent in the parallel shock (34). Alfvén discontinuity (32), in turn, leaves the plasma internal energy unchanged because $\{\rho\} = 0$ there. To determine the efficiency of plasma heating due to discontinuous flows of other types, information about the magnetic field configuration is required.

4.2 Heating dependence on the discontinuity type

Equation (47) allows making certain general conclusions about the internal energy change of the plasma across the discontinuity surface. First, the internal energy of the plasma increases because $-\{r\} > 0$ according to the Zemplén theorem, and $\tilde{p}$ and $\{B_y\}^2$ are positive quantities. Second, the change in the internal energy consists of two parts: a thermodynamic one depending on the plasma pressure and a magnetic one related to the magnetic field structure change near the discontinuity surface.

We consider the adiabatic approximation $p \sim \rho^\gamma$, where γ is the adiabatic index. The thermodynamic part of the internal energy jump increases with the density jump at the discontinuity:

$$\{\epsilon\} = -\{r\}\tilde{p} \sim \{\rho\}^\gamma.$$

The character of the dependence on ρ_1 is determined by the adiabatic index γ, namely,

$$\{\epsilon\} = -\{r\}\tilde{p} \sim \rho_1^{\gamma-2}.$$

For an ideal gas, $\gamma = (i+2)/i$, where i is the number of degrees of freedom of plasma particles (see [76]). The internal energy jump increases with ρ_1 for $\gamma > 2$ ($i < 2$) and decreases for $\gamma < 2$ ($i > 2$). The number of degrees of freedom therefore affects the heating of matter.

The magnetic part of the internal energy jump depends on the magnetic field configuration and hence on the discontinuity type. To use the relations between the magnetic field inclination angles obtained above (see Fig. 6), we transform Eqn (48):

$$\{\epsilon\} = -\{r\}\tilde{p} - \{r\}\frac{\{B_y\}^2}{16\pi} = -\{r\}\tilde{p} - \{r\}\frac{B_x^2}{16\pi}\frac{\{B_y\}^2}{B_x^2} = -\{r\}\tilde{p} - \{r\}\frac{B_x^2}{16\pi}(\tan\theta_2 - \tan\theta_1)^2.$$

The thermodynamic part of the heating, which is independent of the discontinuity type, is referred to as the zero point, and the internal energy jump itself is measured in units of $-\{r\}B_x^2/16\pi$. For this, we make the substitution

$$\{\epsilon\}' = -\frac{16\pi}{\{r\}B_x^2}\left(\{\epsilon\} + \{r\}\tilde{p}\right).$$

We obtain the equation

$$\{\epsilon\}' = (\tan\theta_2 - \tan\theta_1)^2. \tag{49}$$

Plots of Eqn (49) for distributions of the angle θ obtained above are presented in Fig. 11.

Similarly to Section 3.1, we find an equation for the curve on which the strongest trans-Alfvénic and fast shocks lie. To do this, we first express $\tan\theta_1$ from Eqn (18) and substitute it in Eqn (49):

$$\{\epsilon\}' = \left(\frac{m^2/m_{\rm off}^2 - m^2/m_{\rm on}^2}{m^2/m_{\rm off}^2 - 1}\tan\theta_2\right)^2. \tag{50}$$

we then substitute expression (25) in the obtained equation:

$$\{\epsilon\}' = \frac{(m^2/m_{\rm off}^2 - m^2/m_{\rm on}^2)^2}{m^2/m_{\rm A}^2 - 1}. \tag{51}$$

The thin line in Fig. 11 shows the plot of curve (51).

Figure 11 implies that the maximum internal energy jump for the given plasma parameters is produced by the strongest trans-Alfvénic shock, with its amplitude strongly increasing with the magnetic field incidence angle θ_1. The relations between the plasma heating efficiency by other types of oblique shocks depend on the specific flow conditions. For example, the heating by slow shocks can be either weaker or stronger than by trans-Alfvénic shocks. To compare the heating by a perpendicular shock with that by the shocks

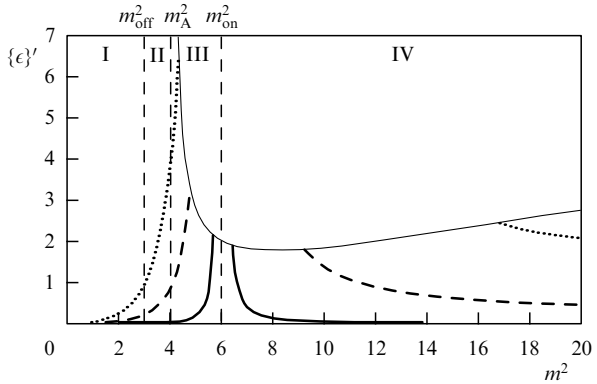

Figure 11. Internal energy jump $\{\epsilon\}'$ as a function of the mass flux across the discontinuity for different values of the angle $\theta_1 = 5°$ (solid curve), 25° (dashed curve), and 45° (dotted curve).

shown in Fig. 11, we take B_x in formula (50) to be equal to the normal field component in oblique shocks, and find the component B_{y1} of the perpendicular shock from the relation $B_{y1} = B_x \tan\theta_1$. The component B_{y2} is determined from formula (27). The heating by oblique shocks corresponds to asymptotes of the plots in Fig. 11 as $m \to \infty$. The internal energy jump at a parallel shock, as was shown in Section 4.1, does not have a magnetic component, and is completely absent at an Alfvén discontinuity. No plasma flow occurs across the contact or tangential discontinuities, and hence there is no plasma heating in these cases.

In any case, the heating amplitude naturally depends on the strength of the shock. The stronger the magnetic energy density changes across the discontinuity, the higher the plasma heating temperature.

5. Properties of a reconnecting current sheet

5.1 Classical models of reconnection

Magnetic reconnection is one of the most important processes in space plasma generating discontinuous flows. It serves as the key mechanism in many astrophysical flaring processes, including flares in coronas of accretion discs around relativistic compact stars (see Section 10.3 in [30]), solar flares [16, 24, 29, 77], and geomagnetic storms [17]. The usual reconnection scenario in application to these phenomena is as follows. Initially, the flare energy is stored in the form of an energy excess of a nonpotential magnetic field compared to the potential field. Then, in the process of reconnection, the magnetic energy excess, i.e., the 'free magnetic energy', is released in the form of thermal and kinetic energy of the plasma and accelerated particles.

The first theoretical description of the magnetic reconnection mechanism was proposed by Sweet and Parker [19, 20] for incompressible plasma in the framework of a stationary two-dimensional MHD problem, whose solution was replaced by an order-of-magnitude analysis of dimensional relations. It may seem that such an approach does not deserve serious attention. However, it is very instructive, and it makes sense to summarize it below (see [13, 78] for more details).

In the Sweet–Parker model, the reconnection proceeds between homogeneous parallel magnetic fields oppositely directed relative to each other. In a thin plasma layer separating these fields, a flat current sheet emerges whose thickness is much smaller than the width. The width of the sheet characterizes the size of the interacting region of the magnetic fluxes and hence their interaction energy. The thickness of the sheet is determined by the plasma conductivity and the inflow velocity. The latter is related to the outflow velocity through the ends of the sheet by the mass conservation law. Thus, the current sheet mediates the reconnection of magnetic field lines. However, estimates of the reconnection rate (see, e.g., [78]) have turned out to be several orders of magnitude smaller than the observed reconnection rate and the corresponding power released in solar flares. What is the reason for this?

The plasma enters the current sheet across its entire width. To accumulate a sufficient amount of the free magnetic energy, the plasma inflow velocity (the reconnection rate) must increase as the width of the current sheet decreases. For a fast reconnection, Petschek proposed a model with a significantly smaller field interaction region [21]. The model describes the reconnection of homogeneous magnetic fields

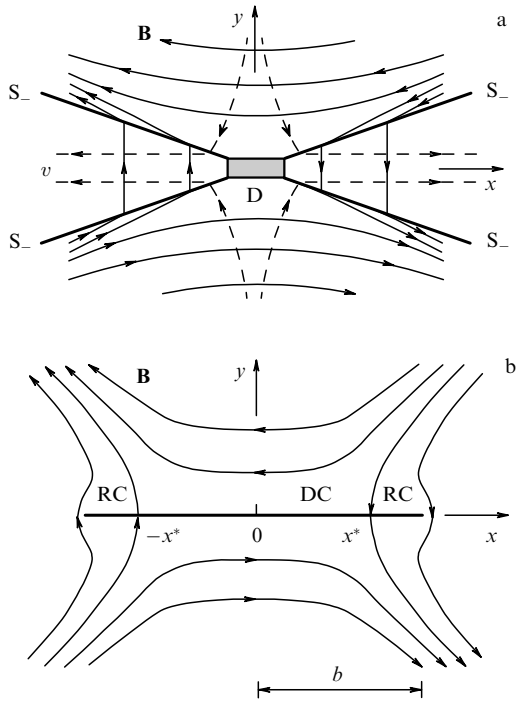

Figure 12. Two classical two-dimensional magnetic reconnection models. (a) The Petschek flow consists of a small diffusion region D and four attached slow shocks S_. (b) Syrovatskii's current sheet includes the direct current region (DC) and two reverse current regions (RC). $2b$ is the width of the current sheet.

(at large distances from the y axis in Fig. 12a) proceeding in a narrow diffusion region D (along the x axis). Most of the magnetic energy transformation into the thermal and kinetic plasma energy occurs outside this region, namely, at four attached slow shocks of infinite length S_.

If there were no shocks, the diffusion region D, i.e., the region of interaction and annihilation of oppositely directed magnetic fields, would have infinite width. In other words, it would be a flat current sheet as in the Sweet–Parker model. The shocks in the Petschek model make the diffusion region width finite. In the ideal MHD approximation, the shocks have zero thickness, i.e., are replaced by discontinuities. The magnetic field outside the discontinuities and the D region is assumed to be potential.

The inclusion of shocks in the model allowed Petschek to increase the expected reconnection rate by two orders of magnitude. Nevertheless, it remained below the observed reconnection rate in solar flares [40] and did not explain the power released. On the other hand, the results of numerical experiments [60] were in qualitative agreement with the Sweet–Parker model. Later, Kulsrud [79] demonstrated that in the homogeneous conductivity approximation (in which the above results were obtained), the diffusion region of the Petschek flow should be of the same size as the Sweet–Parker current sheet and should therefore have the same reconnection rate. He also noted that the use of an inhomogeneous conductivity can increase the reconnection rate in both models to values observed in astrophysical conditions [80]. Unfortunately, the Petschek model has some internal contradictions, which show up in the case of reconnection in highly conductive plasmas, which is the most interesting from the astrophysical standpoint (see Section 6.3 in [13]). In addition, the magnetic reconnection theory is constantly being

improved by taking significant physical effects into account, such as radiation energy losses [81, 82], viscous heating, energy redistribution by thermal conductivity, and MHD turbulence [30, 83, 84]. A discussion of these factors, however, is beyond the scope of this paper.

Here, we mostly consider another classical model of magnetic reconnection, the reconnection in the Syrovatskii thin current sheet. Unlike the Petschek and Sweet–Parker models and their modifications, such a sheet is formed in the vicinity of a zero of a hyperbolic magnetic field. This provides a more precise description, for example, of the pre-flare configuration of magnetic fields in the solar corona. Syrovatskii formulated an analytic model of the reconnecting current sheet in the strong-field and cold-plasma approximation [26].

The current sheet in the Syrovatskii model is a flat surface of finite width separating oppositely directed magnetic fields, as shown in Fig. 12b. The internal structure of this discontinuity assumes a two-dimensional reconnection in a neutral sheet [25], i.e., in the sheet where the normal (perpendicular) component of the magnetic field is absent. The transition to the zero-thickness current sheet is possible because in highly conducting plasmas, the thickness of the sheet, $2a$, is much smaller than its width $2b$. The points x^* and $-x^*$ separate the direct current region DC from the reverse current region RC.

We note that the neutral Syrovatskii current sheet is fundamentally different from the diffusion region in the Petschek flow models [27]. First, the current density is minimal in the diffusion region, but it is maximal in the center of the current sheet. This fact is significant from the standpoint of stability of the current sheet and the possibility of its disruption. Second, as the plasma conductivity increases, the diffusion region width decreases, while, conversely, the width of the current sheet increases. This allows the free magnetic energy, i.e., the energy of the reconnecting magnetic fluxes (or, in other words, the energy of the current sheet), to accumulate before the flare. Due to these two features, the Syrovatskii current sheet is preferred to the Petschek flow from the standpoint of the reconnecting theory of flares in highly conducting plasmas.

For a current sheet emerging from a low-order zero point, an analytic solution was obtained by the conformal transformation method [26]. Let h_0 be the magnetic field gradient in the vicinity of a zero point in the (x, y) plane considered as the complex plane $z = x + \mathrm{i}y$. Then the solution for the potential magnetic field outside the current sheet is expressed in terms of the complex potential:

$$F(z,t) = A(x,y,t) + \mathrm{i}A^+(x,y,t) = \frac{h_0}{2}\, z\sqrt{z^2-b^2} - \frac{2I}{c}\ln\frac{z+\sqrt{z^2-b^2}}{b} + A_0(t)\,. \quad (52)$$

The magnetic field vector has the form

$$\mathbf{B} = B_x + \mathrm{i}B_y = -\mathrm{i}\left(\frac{\mathrm{d}F}{\mathrm{d}z}\right)^*, \quad (53)$$

where the asterisk denotes complex conjugation.

In the complex z plane, the potential has a singularity in the form of a cut with ends at the points $x = b$ and $x = -b$. On this cut, the surface density of the electric current is

$$j(x) = \frac{ch_0}{2\pi}(b^2 - x^2)^{1/2}$$

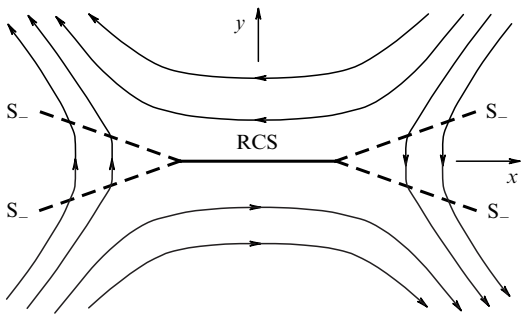

Figure 13. Split current sheet with four attached MHD discontinuities — slow shocks (S_).

if we assume a quasi-stable, fully equilibrium regime of reconnection without reverse currents in the current sheet. The current density $j(x) = 0$ at $x = b$ and $x = -b$. In this particular case, the total current in the sheet is

$$I = \frac{1}{4}\, ch_0 b^2\,. \quad (54)$$

The function $A_0(t)$ corresponds to the magnetic flux dissipated in the current sheet within the time t.

General solution (52) with an arbitrary value of the total current I in the reconnecting current sheet leads to an infinite magnetic field at the current sheet ends. The plasma velocity and density fields in a close vicinity of the current sheet were found in the strong-field and cold-plasma approximation [85]. The features of the plasma flow and density behavior near the reconnecting current sheet explain the origin of the reverse currents. In addition, they play an important role in the current sheet stability. For a given total current, the velocity of electrons increases as the plasma density decreases inside the layer. Various instabilities arise in this way.

Numerical simulations demonstrate the splitting of the reconnecting current sheet (RCS) into different MHD discontinuities [56, 59, 60, 86, 87]. The system of attached discontinuities is frequently found to be much more complicated than that in the Petschek model. Both slow [59, 60] and, for example, fast [86] shocks can be attached to the ends of the current sheet (Fig. 13). At the same time, in theoretical interpretations of numerical models [88], fast and slow shocks are considered to be a possible result of current sheet splitting. In addition, other types of MHD discontinuities are formally not forbidden.

The current sheet splitting process means a change in the magnetic reconnection regime, because the electric field distribution becomes two-dimensional. The reason for this could be the nonevolutionarity of the reconnecting current sheet representing an MHD discontinuity or its structural instability. We consider the conditions under which the splitting occurs.

5.2 The notion of evolutionarity

A stable discontinuity can exist in real plasmas only if it is stable with respect to a decay into other discontinuities or the transition to some nonstationary flow. Let MHD quantities be subjected to an infinitely small perturbation at the initial instant of time. Linear waves then start propagating from the discontinuity. If the amplitudes of these waves and the displacement of the discontinuity are determined from linearized boundary conditions, the problem of the evolution of the initial perturbation with time has a unique solution. If

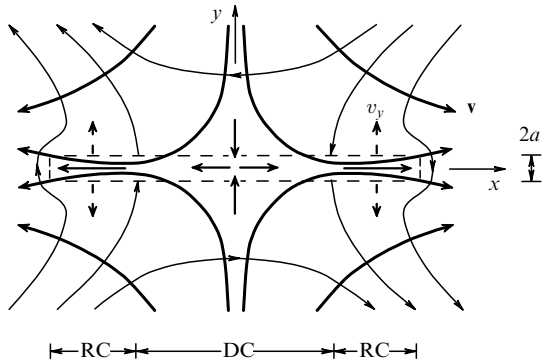

Figure 14. Plasma flows inside the current sheet and its surroundings.

this problem does not have a unique solution, the assumption on the smallness of the initial perturbation is incorrect. In that case, infinitesimal perturbations instantly (in the ideal medium approximation) lead to large nonlinear changes in the initial discontinuous flow. Such a discontinuity is nonevolutionary. We note that, unlike the nonevolutionary discontinuity, the perturbation in an unstable evolutionary discontinuity remains small within a short time interval.

The criterion for evolutionarity results from a comparison of two numbers. The first, N_w, is the number of independent parameters (the amplitudes of outgoing, i.e., reflected and refracted waves, and the displacement of the perturbed discontinuity) describing an infinitesimal perturbation. We recall that the variations of all quantities in each wave are linked by certain relations. Therefore, each wave is determined by one parameter, the amplitude of some quantity. The second number, N_e, is the number of independent boundary conditions (i.e., the number of equations) expressing the unknown parameters in terms of the amplitudes of incident waves. If these numbers are equal, the discontinuity satisfies the evolutionarity requirement. Otherwise, the problem of time evolution of an initially infinitesimal perturbation has no solution or an infinite number of solutions. Such a discontinuity cannot exist in real media and is said to be a nonevolutionary discontinuity.

Because the propagation direction of a wave depends on the relation between its group velocity and the flow velocity, the evolutionarity requirement imposes constraints on the unperturbed MHD quantities on each side of the discontinuity. In particular, shocks turn out to be evolutionary when the upstream and downstream flow velocities either exceed the Alfvén velocity (fast shocks) or are smaller than it (slow shocks).

The reconnecting current sheet cannot be reduced to a one-dimensional flow, because the velocity inhomogeneity inside it is two-dimensional and is characterized by two spatial parameters. The thickness of the sheet, i.e., the distance $2a$ between the reconnecting magnetic fluxes (Fig. 14), determines the magnetic field dissipation rate, and the width $2b$ characterizes the magnetic energy stored in the interaction region. The problem of the evolutionarity of a reconnecting current sheet can be solved only for perturbations interacting with the current sheet as a discontinuity.

5.3 Magnetic field and plasma flows near the current sheet
We consider a thin current sheet arising in the immediate vicinity of the zero magnetic field line of hyperbolic type:

$$\mathbf{B}_0 = (h_0 y, h_0 x, 0)\,.$$

The current sheet is formed by the electric field

$$\mathbf{E} = (0,\, 0,\, E)\,,$$

which is nonzero and is parallel to the zero magnetic field line coinciding with the z axis of a Cartesian coordinate system. The magnetic field lines, frozen into the plasma, flow into the sheet together with the plasma along the y axis. Here, the magnetic field freezing conditions are violated, and the magnetic field lines reconnect in the current sheet and are expelled from it along the x axis. In [26], a simple analytic formula is presented for the distribution of the magnetic field **B** outside the sheet in a complex form in the limit case where the half-thickness of the sheet a (the size along the y axis) is zero (Fig. 12b):

$$B_y + \mathrm{i}B_x = h_0\bigl(\zeta^2 - (x^*)^2\bigr)\bigl(\zeta^2 - b^2\bigr)^{-1/2} \tag{55}$$

(see also [85]). Here, $\zeta = x + \mathrm{i}y$ is a complex variable and b is the half-width of the sheet (the size along the x axis). The quantity I (the total current in the sheet) varies within the range $0 \leqslant I \leqslant ch_0 b^2/4$, where c is the speed of light. At the points

$$x^* = \pm\sqrt{\frac{1}{2}\,b^2 + \frac{2I}{ch_0}}\,, \tag{56}$$

the magnetic field changes sign (see formula (55) and Fig. 12b). The thin sheet approximation means that $a \ll b$.

In the region $|x| < |x^*|$, the directions of the electric current **j** and the electric field in the sheet coincide. This is the direct current, DC, shown in Fig. 12b. However, in regions $|x^*| < |x| < b$, the current is oppositely directed (see the reverse current, RC, in Fig. 12b). If $x \sim b$ and $b - |x^*| \sim b$, the reverse current amplitude is comparable to that of the direct current. We assume that exactly this configuration is realized. Here, all MHD quantities outside the reconnecting current sheet can be considered quasi-homogeneous everywhere except some neighborhoods of the points $x = x^*$ and $x = \pm b$, which are excluded from further consideration without affecting the generality of our conclusions.

Under the assumption of the infinite plasma conductivity σ, b increases without a bound as time progresses. If σ is large but bounded, a finite width $2b$ of the sheet is established in a finite time interval [27] and $a/b \neq 0$, although $a \ll b$. In this case, unlike (55), the transverse magnetic field component $B_y \neq 0$ on the surface and inside the current sheet. However, when the conductivity σ is sufficiently large, $B_x \gg B_y$ outside some neighborhoods of points (56). Further, the component B_y is assumed to be zero on the surface and inside the current sheet, which corresponds to the neutral current sheet approximation. A more general setting of a self-consistent MHD problem of the structure and shape of a reconnecting current sheet that is not magnetically neutral is given in [29], Section 3.4. Below, we restrict ourselves to some qualitative considerations.

Let the plasma flow satisfy the MHD approximation. If $a \ll b$, all variables except the velocity **v** are quasi-homogeneous along the x axis within the sheet. The velocity inhomogeneity is two-dimensional because the mass conservation law at the point $x = 0$, $y = 0$ yields

$$\frac{\partial v_x}{\partial x} = -\frac{\partial v_y}{\partial y}$$

by the flow symmetry. Therefore, the reconnecting current sheet cannot be reduced to a one-dimensional flow. This is obvious because the reconnecting magnetic fluxes move toward each other, and the plasma flow inside the current sheet also must be two-dimensional. In the case of an infinite electric conductivity, the current sheet turns into a tangential discontinuity in the process of formation, formally in the limit $t \to \infty$, where t is the time from the instant of the appearance of the electric field $\mathbf{E}$ in the vicinity of the hyperbolic magnetic field $\mathbf{B}_0$.

We consider a steady current sheet. The electric field $\mathbf{E}$ does not depend on time. Then the aspect ratio a/b can be estimated from the stationary Ohm's law [27] as

$$\frac{a}{b} \sim \frac{\nu_m h_0}{cE}\,, \tag{57}$$

where ν_m is the magnetic viscosity. In addition, in the steady model, the electric field is independent of the coordinates. Therefore, the plasma flows into the sheet in the direct current region, and is expelled from it in the reverse current region.

This pattern of the flow is shown schematically in Fig. 14. The velocity component v_y changes sign when the plasma flows from the direct current region into two reverse current regions (the same regions as in Fig. 12b). This is important in order to calculate the number of outgoing low-amplitude waves N_w.

5.4 Necessary assumptions

We suppose that all dissipative factors except the magnetic viscosity ν_m are zero and ν_m is so small that

$$\frac{cE}{h_0 b} \ll \frac{h_0 b}{\sqrt{4\pi\rho}}\,. \tag{58}$$

The left-hand side of this inequality is a characteristic drift velocity directed toward the current sheet v_y, while the right-hand side coincides with the Alfvén velocity V_A.

We also assume that

$$\rho^{in} \sim \rho^{ex}\,, \tag{59}$$

where the indices 'in' and 'ex' refer to internal and external quantities for the sheet. Such a relation between the plasma densities is found, for example, in the numerical experiment in [59].

For an infinite electric conductivity σ, the magnetic field on the surface of the current sheet grows unboundedly with time, and the drift velocity near the sheet tends to zero. This corresponds to the absence of reconnection in ideal plasmas. At the same time, the pressure p outside the reconnecting current sheet is close to its value at $\zeta = \infty$ and is nonzero or infinite for any σ. From this, we can conclude that for a sufficiently high conductivity, outside the vicinity of point (56), the sound velocity V_s satisfies the condition

$$v_y^{ex} \ll V_s^{ex} \ll V_A^{ex}\,. \tag{60}$$

Inequalities (60) are in good agreement with the magnetostatic approximation.

Taking the characteristic values of these quantities for an active region in the solar corona,

$$v_y \sim 10 \text{ km s}^{-1}\,, \quad V_s \sim 100 \text{ km s}^{-1}\,, \quad V_A \sim 1000 \text{ km s}^{-1}\,,$$

we see that approximation (60) is applicable there.

As regards the velocity component v_x inside the current sheet, its modulus increases from zero at $x = 0$ to

$$|v_x^{in}| \sim \frac{h_0 b}{\sqrt{4\pi\rho}} \tag{61}$$

at $x = x^*$ [26] and then decreases to zero toward $|x| = b$. Outside the current sheet, the velocity component v_x is also not greater than the characteristic Alfvén velocity.

We suppose that the set of MHD quantities Q is subjected to a small perturbation δQ. For simplicity, we set

$$\delta v_z \equiv 0\,, \quad \delta B_z \equiv 0$$

and assume that the perturbation satisfies the WKB approximation conditions outside the current sheet [68]. For an interaction of such perturbations with the current sheet as with a discontinuity, at least two conditions must be satisfied. First, the perturbation wavelength must be much longer than the current sheet thickness, i.e., the wave vector must obey the inequality $k_y \ll a^{-1}$. If the opposite inequality holds, wave diffraction instead of reflection and refraction would occur on scales of the order of a. However, a second condition is also important. Perturbations inside the sheet must be described by ordinary differential equations in y. Otherwise, the perturbation would depend on two variables, and one-dimensional boundary conditions on the current sheet surface would not be satisfied. Therefore, another small parameter, $1/kb$, should exist. We take this parameter as the main and the only one because $b \gg a$. Then the situation is greatly simplified (see [57]).

In the zeroth order in the small parameter $1/kb$, the wave vector $\mathbf{k}$ can be determined from the dispersion equation

$$\omega_0\left[\mathrm{i}k^2 V_s^2(\mathbf{k}\mathbf{V}_A)^2 - V_s^2 k^2 \omega_0(\mathrm{i}\omega_0 - \nu_m k^2) - \mathrm{i}k^2 V_A^2 \omega_0^2 + \omega_0^3(\mathrm{i}\omega_0 - \nu_m k^2)\right] = 0\,, \tag{62}$$

where $\omega_0 = \omega - \mathbf{k}\mathbf{v}$ is the frequency in the plasma rest frame.

In addition to the above assumptions, we impose the following restrictions on the frequency ω in the 'laboratory' frame where the current sheet is at rest:

$$\frac{v_y}{a} \ll \omega_\parallel \ll \frac{V_s}{a}\,, \tag{63}$$

with

$$\omega_\parallel = \omega - k_x v_x\,. \tag{64}$$

The right-hand inequality in (63) means that weak-amplitude sound waves satisfy the condition $k_y \ll a^{-1}$. The left-hand inequality allows reducing the equations for perturbations inside the sheet to ordinary differential equations with respect to y.

As an example, we consider the linearized mass conservation equation

$$\frac{\partial\delta\rho}{\partial t} + \delta\rho\,\frac{\partial v_x}{\partial x} + \rho\,\frac{\partial\delta v_x}{\partial x} + \delta v_x\,\frac{\partial\rho}{\partial x} + v_x\,\frac{\partial\delta\rho}{\partial x} + v_y\,\frac{\partial\delta\rho}{\partial y} + \delta\rho\,\frac{\partial v_y}{\partial y} + \delta v_y\,\frac{\partial\rho}{\partial y} + \rho\,\frac{\partial\delta v_y}{\partial y} = 0\,. \tag{65}$$

If $a \ll c$, the derivative $\partial\rho/\partial x$ inside the current sheet can be neglected. Because the plasma flow is two-dimensional and the velocity inside the reconnecting current sheet is not

uniform, terms with $\partial v_y/\partial y$ should be neglected together with terms proportional to $\partial v_x/\partial x$.

Thus, with (60) taken into account, the problem contains the following small parameters:

$$\varepsilon_0 = \frac{v_y^{\rm ex}}{a\omega_{\parallel}^{\rm ex}}\,, \quad \varepsilon_1 = \frac{a\omega_{\parallel}^{\rm ex}}{V_{\rm s}^{\rm ex}}\,, \quad \varepsilon_2 = \frac{v_y^{\rm ex}}{V_{\rm s}^{\rm ex}}\,, \quad \varepsilon_3 = \left(\frac{V_{\rm s}^{\rm ex}}{V_{\rm A}^{\rm ex}}\right)^2 . \tag{66}$$

For simplicity, we additionally set

$$v_y \sim \frac{V_{\rm s}^3}{V_{\rm A}^2}\,. \tag{67}$$

It is this velocity component that enters the criterion of the current sheet evolutionarity.

We now consider infinitesimal perturbations of the reconnecting current sheet using the plasma flow features described above.

6. Evolutionarity of the reconnecting current sheet

6.1 Perturbations normal to the current sheet

First, we consider the case of perturbations propagating along the normal to the current sheet, i.e., with $k_x = 0$. In the zeroth order in the small parameters defined by inequalities (63), solutions of Eqn (62) are

$$k_y^{\rm d} = -{\rm i}\,\frac{v_y}{\nu_{\rm m}}\,\frac{V_{\rm A}^2}{V_{\rm s}^2}\,, \tag{68}$$

$$k_y^0 = \frac{\omega}{v_y}\,, \tag{69}$$

$$k_y^- = \frac{\omega}{v_y}\,, \tag{70}$$

$$k_y^+ = \pm\frac{\omega}{V_{\rm A}}\,. \tag{71}$$

Here, root (71) is double-valued.

Perturbations satisfy the WKB approximation (see [68]) if

$$\frac{1}{k_y^+ b} \ll 1\,,$$

where $|k_y^+|$ is the smallest wavenumber. This condition is equivalent to the following condition for the frequency ω:

$$\omega \gg \frac{h_0}{\sqrt{4\pi\rho}}\,. \tag{72}$$

If condition (72) holds, derivatives of the unperturbed quantities with respect to coordinates can be neglected in linear MHD equations, and dispersion equation (62) is satisfied.

To obtain the condition for evolutionarity, we must divide the perturbations into those coming to the current sheet and those going out from it. As a rule, such a division should be done according to the sign of the sum of projections of the flow velocity **v** and the group velocity on the normal of the current sheet. However, in the case of normal propagation, it suffices to determine the sign of the phase velocity, because in the absence of frequency dispersion that velocity coincides with the group velocity projection on the direction of the vector **k** in the plasma rest frame [89].

A perturbation with the wavevector k_y^0 from Eqn (69) corresponds to an entropy wave, and k_y^- from solution (70) corresponds to a slow magnetoacoustic wave propagating across the magnetic field. In the plasma rest frame, their phase velocities are zero, but in the laboratory frame they coincide with the plasma velocity **v**. If this is the case, both perturbations move toward the current sheet when the plasma flows into it and move out of the layer when the plasma flows out from it. In addition, for the left-hand side of inequality (69), we have

$$k_y^0 \gg \frac{1}{a}\,, \quad k_y^- \gg \frac{1}{a}\,.$$

Therefore, the reconnecting current sheet is not a discontinuity for perturbations (69) and (70).

Perturbations with the vector k_y^+ from solution (71) are fast magnetoacoustic waves. Their phase velocities ω/k_y^+ satisfy the condition $V_{\rm ph}^+ \gg v_y$ [see (60) and (71)] and are directed along the normal to the current sheet or away from it. One of the waves always enters the layer, irrespective of the sign of v_y. Unlike the case with k_y^0 and k_y^-, we have $k_y^+ \ll 1/a$, and waves (71) interact with the reconnecting current sheet as with a discontinuity.

The perturbation $k_y^{\rm d}$ from solution (68) is a dissipative wave. It decays at distances much shorter than the current sheet half-thickness a. Therefore, as was noted in [75], the amplitude of this perturbation does not appear in the boundary conditions on the discontinuity surface. Dissipative effects outside the current sheet are insignificant.

Thus, in the case of normal propagation, there is one outgoing shock from each side of the current sheet where the plasma flows into it (in the direct current region), and there are four shocks where the plasma flows out from the sheet (in the reversed current region).

6.2 Oblique propagation of perturbations

We now turn to oblique propagation of waves. To solve the problem of evolutionarity of the current sheet as a discontinuity, it is necessary to obtain a solution of Eqn (62) for arbitrary ω and k_x. As shown in [89], for a given flow, the number of shocks propagating from the x axis with arbitrary ω and k_x does not depend on k_x, i.e., on the propagation angle [90]. Hence, it suffices to determine the number of such shocks for $k_x = 0$. From Section 5.3, it follows that when the plasma flows into the sheet (the direct current region in Fig. 12b), there is only one outgoing shock on each side from it. However, when the plasma flows out from the sheet, there are four such shocks.

In a reconnecting current sheet under condition (63), the number of perturbations with $k_y \ll 1/a$ depends on k_x. If $k_x = 0$, there can be two such perturbations determined by the wavevector k_y^+ from (71). As we show below, there are three outgoing perturbations for oblique propagation. This fact is important for further considerations.

The wavevector of a slow magnetoacoustic wave is given by

$$|\mathbf{k}^-| = \frac{\omega}{v_y \sin\theta + v_x \cos\theta \pm |V_{\rm ph}^-|}\,, \tag{73}$$

where $V_{\rm ph}^-$ is the phase velocity and θ is the angle between the wavevector $\mathbf{k}^-$ and the x axis. The scalar product **kv** is here

represented in the form

$$\mathbf{kv} = |\mathbf{k}^-|(v_y \sin\theta + v_x \cos\theta)\,.$$

For $V_s \ll V_A$, the following expression for $|V_{ph}^-|$ holds:

$$|V_{ph}^-| = \frac{V_A V_s}{V_\perp}|\cos\theta|\left[1+\frac{1}{2}\frac{V_A^2 V_s^2}{V_\perp^4}\cos^2\theta + o\left(\frac{V_A^2 V_s^2}{V_\perp^4}\right)\right], \quad (74)$$

where $V_\perp^2 = V_A^2 + V_s^2$.

We choose the angle θ_0 such that $|V_{ph}^-| \sim V_s$, i.e., the value $|\cos\theta_0|$ is not small, and find solutions of (62) for fixed values of ω and

$$k_x = |\mathbf{k}^-|\cos\theta_0\,. \quad (75)$$

For this, we isolate the unknown variable k_y:

$$\begin{aligned}(\omega_\parallel - k_y v_y)\Big[&(\nu_m v_y V_s^2)\,k_y^5 + (\mathrm{i}v_y^2 V_\perp^2 - \nu_m \omega_\parallel V_s^2)\,k_y^4\\ &- (2\mathrm{i}\omega_\parallel v_y V_\perp^2)\,k_y^3 + \mathrm{i}(\omega_\parallel^2 V_\perp^2 - k_x^2 V_A^2 V_s^2)\,k_y^2\\ &- \left[2\mathrm{i}\omega_\parallel v_y (V_\perp^2 k_x^2 - 2\omega_\parallel^2)\right]k_y\\ &+ \mathrm{i}k_x^2(\omega_\parallel^2 V_\perp^2 - k_x^2 V_A^2 V_s^2) - \mathrm{i}\omega_\parallel^4\Big] = 0\,. \end{aligned} \quad (76)$$

Condition (63) was used here.

In the zeroth order in the small parameters defined by the inequality in (63), this equation has the following solutions: the dissipative wave (68) and

$$k_y^0 = \frac{\omega_\parallel}{v_y}\,, \quad (77)$$

$$k_y^{1-} = \frac{2\omega_\parallel}{v_y}\,, \quad (78)$$

$$k_y^{2-} = k_x \tan\theta_0\,, \quad (79)$$

$$k_y^s = \frac{1}{2}\left[\frac{\omega_\parallel V_s^2\cos^2\theta_0}{2v_y V_A^2} \pm \left(-\frac{4\omega_\parallel^2}{V_s^2} + \frac{\omega_\parallel^2 V_s^4\cos^4\theta_0}{4v_y^2 V_A^4} \pm 2\sin\theta_0|\cos\theta_0|\,\frac{\omega_\parallel^2 V_s}{v_y V_A^2}\right)^{1/2}\right]. \quad (80)$$

The sign inside the parentheses in (80) coincides with that before $|V_{ph}^-|$ in formula (73), and the sign before the parentheses defines two different solutions of Eqn (76). Inequality (63) implies that for perturbations (77) and (78), $k_y \gg 1/a$, but for (79) and (80), conversely, $k_y \ll 1/a$.

Perturbations with k_y^{1-} and k_y^{2-} are slow magnetosonic waves, where the angle that the wavevector $\mathbf{k}^{2-}$ makes with the x axis is equal to θ_0 from expression (75) for k_x. Perturbations with k_y^s can be either slow magnetosonic or surface waves, depending on the ratio $v_y V_A^2/V_s^3$.

If the expression inside the parentheses in formula (80) is negative, k_y^s has an imaginary part. The corresponding perturbations exponentially grow or decay at a characteristic distance that is much shorter than a.

The analysis of the second-order polynomial in v_y in the parentheses in Eqn (80) shows that it is equal to zero at the points

$$v_y = \frac{V_s^3}{4V_A^2}|\cos\theta_0|\,(\pm\sin\theta_0 \pm 1)\,. \quad (81)$$

Here, the sign before $\sin\theta_0$ is determined by the sign in (73). The two signs before unity determine two values on the y axis between which perturbations (80) are magnetosonic waves. Outside this interval, they become surface waves. Perturbations that increase in propagating away from the current sheet surface must be excluded because they do not satisfy the boundary condition at infinity. As shown in [89], decaying perturbations are those that leave the discontinuity surface.

Below, we use the fact that at sufficiently high velocities v_y, perturbations (80) are surface waves, irrespective of the values of θ_0. It can be shown that the function $v_y(\theta_0)$ defined by (80) is bounded in absolute value from above by

$$v_y^{\max} = \frac{3\sqrt{3}}{16}\frac{V_s^3}{V_A^2}\,. \quad (82)$$

The maximum in (82) is reached at $\theta_0 = \pi/6$. If

$$|v_y| > v_y^{\max}\,, \quad (83)$$

perturbations (80) are surface waves for any θ_0.

A surface perturbation decaying with the distance from the x axis does not transport energy from the current sheet surface, because its amplitude vanishes at $y = \infty$. However, this surface wave is included in the total perturbation of the reconnecting current sheet, and its amplitude must be determined from the boundary conditions. According to this property, the surface wave is classified as an outgoing wave.

As regards the growing perturbations, they are formally incoming waves, but they must be rejected because their amplitude tends to infinity as $y \to \infty$. For this reason, in the plasma outflow region from the current sheet where only one incoming wave is possible, incoming waves are absent for a given θ_0 when $|v_y| > v_y^{\max}$.

We note that $v_y^{\max}$ coincides with the maximal value of the projection of the slow magnetosonic wave group velocity on the y axis, which in the approximation $V_s \ll V_A$ has the form

$$(V_{gr}^-)_y = \frac{V_s^3}{V_A^2}\sin\theta\cos^3\theta\,. \quad (84)$$

In addition, this value is also attained at the angle $\theta = \pi/6$. For example, inequality (83) means that all slow magnetosonic waves are either incoming or outgoing, depending on the plasma flow direction, towards or away from the current sheet.

To solve the problem of the evolutionarity of a reconnecting current sheet, we must specify appropriate boundary conditions. They relate the amplitudes of perturbations for which $k_y \ll 1/a$ (i.e., the perturbations interacting with the current sheet as with a discontinuity) on each side of the current sheet surface. However, this is not a simple task. Unlike one-dimensional discontinuities, waves with $k_y \ll 1/a$ outside the current sheet can give rise to perturbations for which the opposite inequality holds inside the current sheet. In addition, because dissipative effects are important inside the current sheet, the wavenumbers of these perturbations have imaginary parts that tend to infinity as $a/b \to 0$. This implies that the amplitude of perturbations increases without a bound. Therefore, linearized one-dimensional boundary conditions are not satisfied as a whole on the reconnecting current sheet [58]. This fact is clarified in the next section when analyzing perturbations inside the current sheet.

6.3 Perturbations inside the current sheet

In the zeroth order in the small parameters ε_i, solutions of Eqn (76) take the form

$$k_y^{\mathrm{d}} = \frac{\omega_\parallel}{v_y}\,, \tag{85}$$

$$k_y^{-} = \pm\sqrt{\frac{\mathrm{i}A}{V_{\mathrm{s}}^2 \nu_{\mathrm{m}} \omega_\parallel}}\,, \tag{86}$$

$$k_y^{*} = \frac{1}{A}\left[\omega_\parallel v_y F \pm \sqrt{\omega_\parallel^2 v_y^2 F^2 - A(k_x^2 A - \omega_\parallel^4)}\right], \tag{87}$$

where

$$F = V_\perp^2 k_x^2 - 2\omega_\parallel^2\,,$$

$$A = \omega_\parallel^2 V_\perp^2 - k_x^2 V_{\mathrm{A}}^2 V_{\mathrm{s}}^2\,.$$

It follows from the main inequality (63) that wave vectors (77), (85), and (86) satisfy the WKB approximation inside the reconnecting current sheet. The dispersion relation is valid for them as long as the terms with derivatives of unperturbed variables in the MHD equations (see [68], Ch. VIII) are insignificant in the limit $k_y \gg 1/a$.

Expressions (85) and (86) yield four solutions of the MHD equations in the WKB approximation. By contrast, perturbations (87) do not satisfy the WKB approximation, because for them $1/k_y a \to 0$. In this case, it is not possible to ignore the derivatives of the unperturbed variables in the MHD equations and to use Eqn (76).

We thus conclude that inside the reconnection current sheet, there are four perturbations that satisfy the WKB approximation irrespective of the value of k_x. We recall that outside the current sheet, there are four such perturbations in the case of normal propagation and three perturbations in the case of oblique propagation. In the latter case, the perturbations with $k_y \ll 1/a$ and $k_y \gg 1/a$ transform into each other.

6.4 One-dimensional boundary conditions

For a specified but sufficiently general distribution of unperturbed MHD parameters inside the reconnecting current sheet, expressions for perturbations (and, hence, describing the transition between perturbations with $k_y \ll 1/a$ and $k_y \gg 1/a$) can be found analytically [58]. These solutions are shown schematically in Fig. 15.

The horizontal solid and dashed lines represent the respective solutions with $k_y \ll 1/a$ and $k_y \gg 1/a$. The slanted lines represent the solutions that do not satisfy the WKB approximation. A superposition of perturbations on one side of the thick vertical line $y = \pm a$ (i.e., on one side of the current sheet) turns into a superposition of perturbations on the other side.

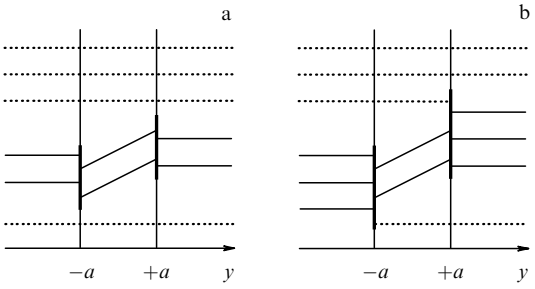

Figure 15. Schematics of the solution of linearized MHD equations in the case of (a) normal and (b) oblique propagation.

In the case of normal propagation, long waves with $k_y \ll 1/a$ do not turn into short waves with $k_y \gg 1/a$ (Fig. 15a). In this case, long waves interact with the reconnecting current sheet as with a tangential discontinuity, i.e., as if the velocity component v_y were zero. The wave amplitudes satisfy the linearized boundary conditions for magnetoacoustic waves at the tangential discontinuity with $v_{x1} = v_{x2}$:

$$\left\{\delta p + \frac{B_x\,\delta B_x}{4\pi}\right\} = 0\,, \qquad \{\delta v_y\} = 0\,. \tag{88}$$

Thus, there are two boundary conditions and two outgoing waves for any sign of v_y. In addition, Eqns (88) always have a unique solution. Therefore, the reconnecting current sheet is evolutionary for normally propagating waves.

Another situation emerges in the case of oblique propagation, where long waves outside the sheet turn into short waves inside the sheet. This imposes two additional boundary conditions on the perturbations that interact with the reconnecting current sheet as with a discontinuity; for such perturbations, the short-wave amplitudes should be zero. As a consequence, the current sheet behaves like a discontinuity only for specially chosen perturbations.

The problem of the evolutionarity of such perturbations can be formulated. However, conclusions about the nonevolutionarity are different for the direct current region, where the plasma flows into the reconnecting current sheet, and for the reverse current regions, where the plasma flows out from the sheet.

6.5 Evolutionarity and decay

We have obtained the evolutionarity criterion for a reconnecting current sheet treated as an MHD discontinuity.

If the plasma flows into the sheet (in the direct current region in Figs 12b or 14) or if inequality (83) holds, the conclusion about the nonevolutionarity cannot be made. In this case, either the current sheet does not behave as a discontinuity or, alternatively, the problem of small perturbations has a unique solution. In the latter case, we can consider the usual linear stability problem. For example, the question about linear tearing instability [91, 92] always exists in application to the central part (the direct current region) of the reconnecting current sheet.

Let the relation opposite to (83) hold,

$$|v_y^{\mathrm{ex}}| < \frac{3\sqrt{3}}{16}\,\frac{V_{\mathrm{s}}^3}{V_{\mathrm{A}}^2}\,. \tag{89}$$

The plasma flows out from the sheet (in the reverse current regions in Figs 12b and 14), with the outflow velocity being smaller than the projection of the group velocity of the slow magnetoacoustic wave normal on the current sheet [see (89)]. Then there is a perturbation for which, first, the boundary conditions on the sheet surface are satisfied and, second, the outgoing wave amplitudes are large compared to the amplitudes of incident waves in the limit $\varepsilon_i \to 0$, i.e., when the plasma conductivity is sufficiently high.

Such a perturbation inside the current sheet is a solution of the system of linearized MHD equations and is characterized outside the sheet by the resonance angle θ_0^* determined from (81). The perturbation is not described by linear

equations, and its time evolution has no unique solution. Therefore, the current sheet is not evolutionary, and the initial perturbation of the MHD flow is not small. The perturbation can represent the splitting of the current sheet into shocks that are observed in numerical experiments [56, 59, 60, 86].

This allows unifying two regimes of magnetic reconnection in current sheets: with or without MHD discontinuities attached to the current sheet ends (see Section 7). Such a unified model can be used to describe nonstationary phenomena in astrophysical plasmas related to the magnetic reconnection process.

7. Problems of interpretation of numerical simulations

7.1 Discontinuities near the magnetic reconnection region

In [54–56], a two-dimensional analytic model of stationary magnetic reconnection in plasma with a strong magnetic field was constructed. The model includes a thin current sheet and four discontinuous MHD flows of finite length R attached to its ends. Figure 16 shows the right-hand side of the current structure; the left-hand side can be constructed symmetrically with respect to the y axis. The plasma flows into the reconnecting current sheet from above and from below and flows out from it to the left and to the right. The specific geometry of the current sheet is defined by its free parameters, depending on astrophysical applications.

Figure 17 shows a particular case of magnetic reconnection ($L = 1$, $R = 1$, the inclination angle of the discontinuity plane to the x axis is 45°), which can be taken as a template when comparing many other possible reconnection regimes. Figure 17 demonstrates that the current sheet is the main result of the solution of the problem in the central part of the reconnection region. The sheet is 'crossed' by two symmetric magnetic field lines; the 'crossing points' (see [93] for more details about their properties) separate the current sheet parts relative to which the field circulation has opposite signs. Thus, in the central part of the reconnection region, a Syrovatskii current sheet indeed emerges, which consists of the direct current and two attached reverse currents.

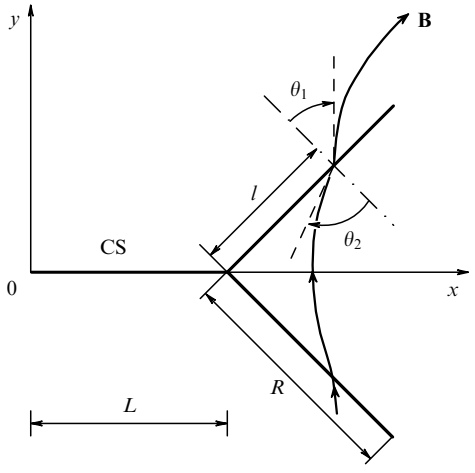

Figure 16. The configuration of electric currents (thick solid segments) consists of the current sheet (CS) and discontinuity surfaces of finite length R attached to its ends; L is the half-thickness of the reconnecting current sheet. The electric currents are parallel to the z axis of a Cartesian coordinate system.

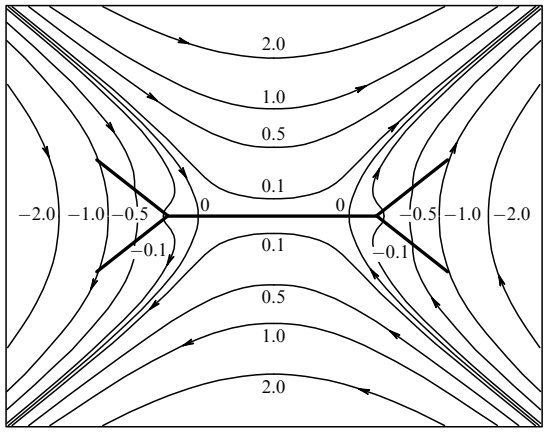

Figure 17. Magnetic field lines (thin curves with arrows) marked with the vector potential values. The direct and reverse current regions are seen inside the current sheet (the horizontal thick solid segment). The magnetic field has a jump at the attached discontinuity surfaces (slanted thick solid segments).

In specific astrophysical applications, in particular, in solar flares, the model of a so-called 'superhot' turbulent current sheet [30] should be used for determining the parameters of this region. An advantage of the analytic model, however, is the possibility of studying general relations independent of the detailed assumptions of the physical model of reconnection. We consider some general properties of discontinuous flows in the vicinity of a current sheet predicted by the analytic model [54, 55]. The magnetic field inclination angles θ_1 and θ_2 are one of the results of the magnetic field calculation (see Fig. 16). Their values change with the coordinate l along the discontinuity surface from the current sheet to the free edge of the shock, which changes the MHD discontinuity type.

In Section 2.3, a graphic representation of the possible dependences between the angles was obtained, as shown in Fig. 5. It can be used to identify the type of discontinuous MHD flows from the known magnetic field configurations in numerical simulations of magnetic reconnection. Indeed, plots of the function $\theta_2 = \arctan(a \tan\theta_1)$ for different values of a do not have crossing points inside the interval $\theta_1 \in (0; \pi/2)$. For this reason, the value of a (and hence the discontinuous flow type) is uniquely defined by the angles θ_1 and θ_2. For $a > 1$, a fast shock emerges. The value $a = 1$ corresponds to a contact discontinuity. If $-1 < a < 1$, a slow shock appears. The value $a = -1$ corresponds to an Alfvén shock. Finally, $a < -1$ corresponds to a trans-Alfvénic shock. The switch-off and switch-on shocks are respectively realized at $a = 0$ and $a \to \infty$. Each value of the coefficient a is determined by three physical parameters ρ_1, ρ_2, and m.

The characteristics of plasma crossing the discontinuity change with the distance from the reconnection point to the current sheet along the discontinuity surface. Different types of discontinuous MHD flows correspond to different flow regimes. Figure 18 shows the gradual change in the magnetic field inclination angles along the attached discontinuity surface starting from the point $l = 0$ of the attachment to the current sheet up to its 'free end' $l = R$, $R = 1$, where the angles θ_1 and θ_2 are equal to each other.

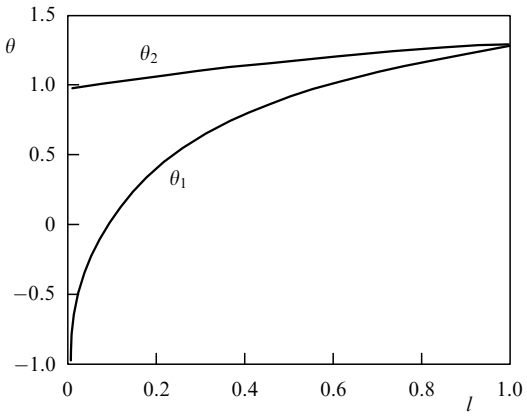

Figure 18. Distribution of the angles θ_1 and θ_2 on the attached discontinuity surface. The variable l is the distance from the current sheet end measured along the discontinuity surface. No slow shocks can be realized in the model.

According to the graphical representation constructed in Section 2.3, near the attachment point of a shock to the current sheet, the shock is trans-Alfvénic. Indeed, the angles θ_1 and θ_2 are different, have opposite signs, and $-\theta_2 > \theta_1$ (Fig. 4d). The situation changes when the angle θ_1 vanishes. At this point, a switch-on shock arises ($\theta_2 \neq 0$). Further, at larger l, the discontinuous flow turns into the fast shock regime. The conditions for this transition are considered in detail in Section 7.2.

In the framework of the same analytic model of reconnection, another distribution of magnetic field inclination angles was also obtained [55], which is characteristic for other model parameters. Figure 19 shows the results of calculations in which 'external' shocks (those that end at free ends of the attached discontinuous flows) are slow. This regime of magnetic reconnection is considered in more detail in Section 7.2. We only note that the presence of slow MHD shocks in the vicinity of the compact reconnecting region is a characteristic feature of the classical Petschek flow [21].

However, we recall that the two-dimensional Petschek flow corresponds to the model problem of reconnection of oppositely directed magnetic fields that are uniform at large distances from the reconnection region, i.e., formally at infinity. At the same time, the analytic model considered here has another asymptotic form of magnetic fields at large distances: the field becomes hyperbolic there. This type of reconnection, apparently, is typical for the case where the reconnecting region (the magnetic field separator in the corona) is not located so high, relatively close to the 'magnetic obstacle', i.e., a flaring loop arcade in the corona [30]. A similar situation arises in a nonstationary MHD model in which the fast reconnection point inside an infinite current sheet is located near a massive slowly moving 'magnetic island' [63].

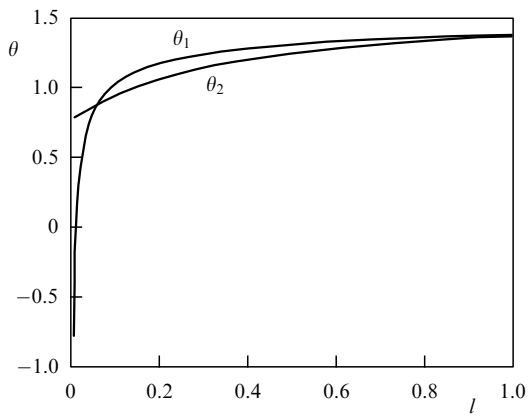

Figure 19. Distribution of angles θ_1 and θ_2 on the attached discontinuity surface. The variable l is the distance from the current sheet end measured along the discontinuity surface. Slow shocks can be realized in the model.

As is well known, trans-Alfvénic shocks are nonevolutionary in both ideal and dissipative MHD [75, 94, 95]. Moreover, they apparently remain nonevolutionary in a weakly collisional magnetized plasma and in the vicinity of superhot turbulent current sheets in solar flares. Hence, we assume that the structure of discontinuous flows becomes more complicated near the ends of such a sheet. It is likely to be similar to the quasistationary picture found in numerical dissipative MHD experiments (see, e.g., [51]). However, a strongly nonstationary picture of discontinuous flows is also possible, which is caused by the so-called oscillatory disintegration of trans-Alfvénic shocks [95].

7.2 Transitions between discontinuities in the reconnection model

The discontinuity surface in Fig. 19, with the behavior of angles on the surface shown there, can be separated into three regions according to the types of discontinuous flows. A trans-Alfvénic shock is attached immediately to the current sheet. In Fig. 19, this region corresponds to negative values of θ_1. Away from the current sheet, a fast shock appears ($\theta_2 > \theta_1$) up to the intersection point of the curves θ_1 and θ_2. The discontinuity ends with a slow shock ($\theta_2 < \theta_1$) smoothly transiting into a continuous flow ($\theta_2 = \theta_1$) at the edge of the discontinuity surface, i.e., at $l = 1$.

The change of the shock type with a gradual change in the flow parameters should occur via transitional discontinuities. In the case considered here, the first transition occurs between the trans-Alfvénic and fast shocks. As shown in Section 3.3, switch-on shock (33) plays the role of a transitional discontinuity. Indeed, we see in Fig. 19 that at the transition point between the trans-Alfvénic and fast shocks, the magnetic field in the incident plasma flow is normal to the discontinuity surface ($\theta_1 = 0$), and in the outgoing plasma flow, the field has a tangential component ($\theta_2 > 0$).

This transition cannot occur only by the gradual change in the mass flux across the discontinuity. Simultaneously, the magnetic field incidence angle should decrease in order to diminish the jump between the allowed mass fluxes for fast and trans-Alfvénic shocks (see Fig. 6). In addition, both trans-Alfvénic and fast shocks satisfy inequality (20). Therefore, to smoothly change the medium parameters, the mass flux of the switch-on shock that mediates the transition, must also satisfy the inequality

$$m_{\mathrm{off}}^2 > m_{\mathrm{A}}^2 + m_{\perp}^2 ,$$

or

$$\frac{B_x^2}{4\pi r_2} > \frac{B_x^2 + \tilde{B}_y^2}{4\pi \tilde{r}} .$$

After simplifying the last expression, we obtain a constraint on the possible change in the magnetic field inclination behind

the discontinuity plane:

$$\tan^2\theta_2 < \frac{2\{\rho\}}{\rho_1}\,. \qquad (90)$$

There is no transition solution for the fast-to-slow shock transformation (the intersection point of plots for θ_1 and θ_2 in Fig. 19). Regions of the allowed mass fluxes for these discontinuity types have no common points (see Fig. 6). Moreover, the crossing of the curves in Fig. 19 suggests the absence of magnetic field jumps at the point separating the fast and slow shocks. Only a contact discontinuity has such a field structure. However, in a fast shock, according to Eqn (26), $\tan\theta_2 \to \tan\theta_1$ only as $\{\rho\} \to 0$. The same condition should have been imposed on the transition solution, if it had existed. Meanwhile, substituting $\{\rho\} = 0$ in the boundary conditions of contact discontinuity (29) leaves the parameters of the medium and magnetic field unchanged. The density, velocity, magnetic field, and pressure jumps at the point considered are zero. There is no discontinuity at the contact point between the fast and slow shocks.

Thus, the discontinuity surface turns out to be physically separated into two regions: the inner part consisting of trans-Alfvénic and fast shocks, and the outer part representing a slow shock. By changing the free parameters of the model, it is possible to obtain the reconnection regime in which the discontinuity ends with a fast shock, and the external part of the discontinuity is entirely absent. This suggests that the inner part of the discontinuity is due to the reconnection process itself and is closely related to the presence of reverse currents at the ends of the current sheet, which is well demonstrated in [54]. At the same time, the outer part of the discontinuity is strongly dependent on the external factors affecting the general topology of current sheets, including the presence or absence of the 'magnetic obstacle' and plasma inhomogeneities outside the reconnection site.

Some analogs of the above conclusions can be found in the results of modern numerical MHD simulations of the fast reconnection process. The nonevolutionarity of trans-Alfvénic and switch-on shocks in the analytic model in [54, 55] points to the discontinuity flow decay into a collection of interacting discontinuities. Calculations of numerical models in this region should be especially accurate. This determines the possibility of correctly interpreting a complicated system of shocks observed near the reverse current regions [49, 51, 52]. In [55], the characteristics of the external part of the discontinuity surface formed by slow shocks depend on the geometry of the analytic model and hence on the reconnection process conditions.

Numerical experiments also suggest that the plasma expelled from the reconnecting current sheet is clumped into so-called 'plasmoids'. As a rule, they are separated from the surrounding plasma by a system of slow shocks. The structure and intensity of the latter depend on the size and density of the 'plasmoids'.

Generally, the relation of the magnetic reconnection processes to the formation of the accompanying discontinuous flows requires further careful investigation.

7.3 Plasma heating outside the reconnection region

The strongest matter heating at the discontinuities can be expected from plasma subjected to a strong density jump in a magnetic field with drastically changing geometry (see Section 4.2). Such conditions hold in the magnetic reconnection region. The merging of two oppositely directed magnetic fluxes results in the formation of a current sheet, which in a highly conducting plasma slows down the reconnection process and accumulates free magnetic energy in its vicinity. This energy is later released during disruption of the current sheet (see, e.g., [24, 30]). Here, the magnetic reconnection mediates the fast transformation of the free magnetic energy into the plasma particle energy and is accompanied by the formation of a complex picture of MHD discontinuities in those regions with sharp changes in the magnetic field and plasma velocities. Such systems of discontinuities are observed in both laboratory and numerical experiments [13, 15].

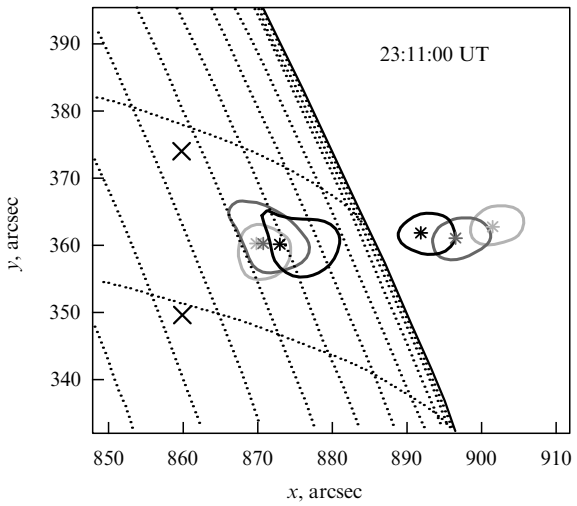

Figure 20. Image of a solar flare obtained by the RHESSI satellite in different energy ranges [45]. The gray level at different closed contours shows the effective temperature range (in keV) (from light to dark): 6–8, 10–12, 14–16 (on the solar disc background), and 10–12, 12–14, 14–16 (outside the limb).

In the analytic model for magnetic reconnection [54, 55], these discontinuous structures are present as separate elements. The types of discontinuities and the transition conditions between different discontinuity types were studied in Sections 7.1 and 7.2. We now briefly discuss the additional plasma heating outside the reconnection region, at the shocks attached to the reconnecting current sheet. First of all, the following facts should be noted. First, near the ends of the current sheet, where the reverse currents are formed, the shocks are trans-Alfvénic. Second, the density jump is large near the current sheet and decreases to zero when approaching the free edge of the discontinuity. In Section 4.2, we showed that all these factors tend to increase the internal energy jump at the discontinuity. Therefore, the most favorable conditions for plasma heating in the reconnection model under consideration are realized near the reverse current region. This is consistent with ideas about the presence of a 'superhot' plasma (with the electron temperature above 10 keV) in solar flares [30].

X-ray observations of solar flares confirm the superhigh plasma temperatures. The temperature increase suggests the presence of the main energy release site (see Fig. 20 in [45]). Modern concepts of the solar flare structure (see [96]) uniquely associate this region with magnetic reconnection. Hard X-ray emission in Fig. 20 shows the location of the 'superhot' plasma passing through a turbulent current sheet. The presence of discontinuous plasma flows at the boundaries

of the high-temperature regions gives rise to additional heating of the plasma passing through the discontinuity.

8. Conclusion

We have presented a review of the modern state of the theory of discontinuous MHD flows and its application to the physics of magnetic reconnection in astrophysical plasmas and in laboratory and numerical studies. The correspondence is established between the standard classification of discontinuous MHD flows [4] and the characteristic plasma flow parameter — the mass flux across the discontinuity, Eqn (18). Transition solutions for all discontinuities with allowed transitions are found in explicit form. They are used to construct a generalized scheme of continuous transitions between discontinuous MHD flows [9]. The scheme includes discontinuities that have not been incorporated in earlier schemes, such as contact discontinuities and switch-on and switch-off shocks. Some types of discontinuous flows, for example, trans-Alfvénic shocks, are nonevolutionary. They are also included in the generalized transition scheme. When interpreting the results of numerical integration of MHD equations, this allows identifying the regions that require more accurate calculations and additional investigation.

The properties of Syrovatskii's reconnecting current sheet are described and the need for generalizing the model in [26] is demonstrated. In the framework of a simplified analytic model [55], it is possible to identify different parts of discontinuous surfaces with different MHD shocks attached to the current sheet. In particular, near the ends of the current sheet (in the presence of reverse currents), the regions of trans-Alfvénic and switch-on shocks, which are known to be nonevolutionary, are located.

Based on the analysis of evolutionarity, the possibility of the current sheet decaying into a system of MHD discontinuities [57] is demonstrated. With the shocks present in the analytic reconnection model in [55] as an example, possible constraints on the flow parameters imposed by the continuous transition conditions are shown. The separation of the discontinuous surfaces attached to the current sheet into two regions of different origins is established. The quasi-stationary inner region is related to the currents in the current sheet, and the outer region is mostly determined by the boundary conditions under which the magnetic reconnection proceeds and by the reconnection rate.

For the analytic equation (47) describing the internal plasma energy change across the MHD discontinuity, its dependence on both thermodynamic plasma parameters and the MHD discontinuity type is found. The larger the plasma density and magnetic energy density jumps at the discontinuity are, the stronger the heating. Trans-Alfvénic flows produce the maximum heating. Such conditions are realized near the reverse current region during magnetic reconnection. The result can be used to explain the plasma temperature distribution in solar flares observed by modern X-ray space observatories [45].

The study was supported by the Russian Foundation for Basic Research (grants 11-02-00843 and 14-02-31425-mol).

References

1. Alfvén H *Cosmic Electrodynamics* (Oxford: Clarendon Press, 1950)
2. De Hoffmann F, Teller E *Phys. Rev.* **80** 692 (1950)
3. Landau L D, Lifshitz E M *Fluid Mechanics* (Oxford: Pergamon Press, 1987); Translated from Russian: *Gidrodinamika* (Moscow: Nauka, 1986)
4. Syrovatskii S I *Usp. Fiz. Nauk* **62** 247 (1957)
5. Polovin R V *Sov. Phys. Usp.* **3** 677 (1961); *Usp. Fiz. Nauk* **72** 33 (1960)
6. Anderson J E *Magnetohydrodynamic Shock Waves* (Cambridge, Mass.: M.I.T. Press, 1963)
7. Syrovatskii S I *Tr. Fiz. Inst. Akad. Nauk SSSR* **8** 13 (1956)
8. Somov B V *Kosmicheskaya Elektrodinamika i Fizika Solntsa* (Cosmic Electrodynamics and Solar Physics) (Moscow: Izd. Mosk. Univ., 1993)
9. Ledentsov L S, Somov B V *JETP* **117** 1164 (2013); *Zh. Eksp. Teor. Fiz.* **144** 1319 (2013)
10. Sutton G W, Sherman A *Engineering Magnetohydrodynamics* (New York: McGraw-Hill, 1965)
11. Luk'yanov S Yu *Goryachaya Plazma i Upravlyaemyi Yadernyi Sintez* (Hot Plasma and Controlled Nuclear Fusion) (Moscow: Nauka, 1975)
12. Morozov A I *Vvedenie v Plazmodinamiku* (Introduction to Plasmadynamics) (Moscow: Fizmatlit, 2006)
13. Biskamp D *Nonlinear Magnetohydrodynamics* (Cambridge, UK: Cambridge Univ. Press, 1997)
14. Imshennik V S, Bobrova N A *Dinamika Stolknovitel'noi Plazmy* (Dynamics of Collisional Plasma) (Moscow: Energoatomizdat, 1997)
15. Büchner J, Dum C T, Scholer M (Eds) *Space Plasma Simulation* (Berlin: Springer, 2003)
16. Giovanelli R G *Nature* **158** 81 (1946)
17. Dungey J W *Cosmic Electrodynamics* (Cambridge: Univ. Press, 1958)
18. Orta J A, Huerta M A, Boynton G C *Astrophys. J.* **596** 646 (2003)
19. Sweet P A, in *Electromagnetic Phenomena in Cosmical Physics* (Proc. IAU Symp., No. 6, Ed. B Lehnert) (Cambridge: Cambridge Univ. Press, 1958) p. 123
20. Parker E N *Phys. Rev.* **107** 830 (1957)
21. Petschek H E, in *The Physics of Solar Flares, Proc. of the AAS-NASA Symp., 28 – 30 October, 1963, Greenbelt, MD* (Ed. W N Hess) (Washington, DC: National Aeronautics and Space Administration, Science and Technical Information Division, 1964) p. 425
22. Hones E W (Jr.) (Ed.) *Magnetic Reconnection in Space and Laboratory Plasmas* (Washington, D.C.: American Geophys. Union, 1984)
23. Hoshino M, Stenzel R L, Shibata K (Eds) *Magnetic Reconnection in Space and Laboratory Plasmas* (Tokyo: Terra Scientific Publ. Co., 2001)
24. Syrovatskii S I *Sov. Astron.* **6** 768 (1963); *Astron. Zh.* **39** 987 (1962)
25. Syrovatskii S I *Sov. Astron.* **10** 270 (1966); *Astron. Zh.* **43** 340 (1966)
26. Syrovatskii S I *Sov. Phys. JETP* **33** 933 (1971); *Zh. Eksp. Teor. Fiz.* **60** 1727 (1971)
27. Syrovatskii S I *Proc. P.N. Lebedev Phys. Inst.* **74** 2 (1976); *Tr. Fiz. Inst. Akad. Nauk SSSR* **74** 3 (1974)
28. Syrovatskii S I *Annu. Rev. Astron. Astrophys.* **19** 163 (1981)
29. Somov B V *Physical Processes in Solar Flares* (Dordrecht: Kluwer Acad. Publ., 1992)
30. Somov B V *Plasma Astrophysics* Pt. II *Reconnection and Flares* 2nd ed. (New York: Springer, 2013)
31. Švestka Z, Jackson B V, Machado M E (Eds) *Eruptive Solar Flares, Proc. of Colloquium No. 133 of the Intern. Astronomical Union, Argentina, 2 – 6 August, 1991* (Berlin: Springer-Verlag, 1992)
32. Hanslmeier A, Veronig A, Messerotti M (Eds) *Solar Magnetic Phenomena, Proc. of the 3rd Summerschool and Workshop, Austria, August 25 – September 5, 2003* (Dordrecht: Springer, 2005)
33. Hanslmeier A *The Sun and Space Weather* (Astrophysics and Space Science Library, Vol. 347) (Dordrecht: Springer, 2007)
34. Kosugi T et al. *Solar Phys.* **136** 17 (1991)
35. Ogawara Y et al. *Solar Phys.* **136** 1 (1991)
36. Tsuneta S et al. *Publ. Astron. Soc. Jpn.* **44** L211 (1992)
37. Tsuneta S *Astrophys. J.* **456** 840 (1996)
38. Masuda S et al. *Nature* **371** 495 (1994)
39. Petrosian V, Donaghy T Q, McTiernan J M *Astrophys. J.* **569** 459 (2002)
40. Yokoyama T et al. *Astrophys. J.* **546** L69 (2001)
41. McKenzie D E, Hudson H S *Astrophys. J.* **519** L93 (1999)
42. Shibata K et al. *Astrophys. J.* **451** L83 (1995)

43. Ohyama M, Shibata K *Astrophys. J.* **499** 934 (1998)
44. Sui L, Holman G D, Dennis B R *Astrophys. J.* **612** 546 (2004)
45. Sui L, Holman G D *Astrophys. J.* **596** L251 (2003)
46. Liu W et al. *Astrophys. J.* **676** 704 (2008)
47. Liu W, Chen Q, Petrosian V *Astrophys. J.* **767** 168 (2013)
48. Shimizu T, Ugai M *Phys. Plasmas* **10** 921 (2003)
49. Shimizu T, Kondoh K, Ugai M, in *Proc. of the Intern. Scientific Conf. on Chromospheric and Coronal Magnetic Fields* (ESA SP-596, Eds D E Innes, A Lagg, S K Solanki) (2005), CD-ROM, 25.1
50. Ugai M, Kondoh K, Shimizu T *Phys. Plasmas* **12** 042903 (2005)
51. Ugai M *Phys. Plasmas* **15** 082306 (2008)
52. Zenitani S, Miyoshi T *Phys. Plasmas* **18** 022105 (2011)
53. Lax P D *Commun. Pure Appl. Math.* **10** 537 (1957)
54. Bezrodnykh S I, Vlasov V I, Somov B V *Astron. Lett.* **33** 130 (2007); *Pis'ma Astron. Zh.* **33** 153 (2007)
55. Bezrodnykh S I, Vlasov V I, Somov B V *Astron. Lett.* **37** 113 (2011); *Pis'ma Astron. Zh.* **37** 133 (2011)
56. Markovskii S A, Somov B V, in *Fizika Solnechnoi Plazmy* (Solar Plasma Physics) (Exec. Eds B V Somov, V V Fomichev) (Moscow: Nauka, 1989) p. 45
57. Markovskii S A, Somov B V *JETP* **77** 253 (1993); *Zh. Eksp. Teor. Fiz.* **104** 2736 (1993)
58. Markovskii S A, Somov B V *J. Plasma Phys.* **55** 303 (1996)
59. Brushlinskii K V, Zaborov A M, Syrovatskii S I *Sov. J. Plasma Phys.* **6** 165 (1980); *Fiz. Plazmy* **6** 297 (1980)
60. Biskamp D *Phys. Fluids* **29** 1520 (1986)
61. Yokoyama T, Shibata K *Astrophys. J.* **474** L61 (1997)
62. Chen P F et al. *Astrophys. J.* **513** 516 (1999)
63. Kondoh K, Ugai M, Shimizu T, in *Proc. of the Intern. Scientific Conf. on Chromospheric and Coronal Magnetic Fields* (ESA SP-596, Eds D E Innes, A Lagg, S K Solanki) (2005), CD-ROM, 72.1
64. Tidman D A, Krall N A *Shock Waves in Collisionless Plasmas* (New York: Wiley-Interscience, 1971)
65. Sirotina E P, Syrovatskii S I *Sov. Phys. JETP* **12** 521 (1961); *Zh. Eksp. Teor. Fiz.* **39** 746 (1960)
66. Zel'dovich Ya B, Raizer Yu P *Physics of Shock Waves and High-Temperature Hydrodynamic Phenomena* (New York: Academic Press, 1966 – 1967); Translated from Russian: *Fizika Udarnykh Voln i Vysokotemperaturnykh Gidrodinamicheskikh Yavlenii* (Moscow: Nauka, 1966)
67. Shercliff J A *A Textbook of Magnetohydrodynamics* (Oxford: Pergamon Press, 1965); Translated into Russian: *Kurs Magnitnoi Gidrodinamiki* (Moscow: Mir, 1967)
68. Landau L D, Lifshitz E M *Electrodynamics of Continuous Media* (Oxford: Pergamon Press, 1984); Translated from Russian: *Elektrodinamika Sploshnykh Sred* (Moscow: Nauka, 1982)
69. Somov B V *Plasma Astrophysics* Pt. I *Fundamental and Practice* 2nd ed. (New York: Springer, 2013)
70. Ledentsov L S, Somov B V*Astron. Lett.* **37** 131 (2011); *Pis'ma Astron. Zh.* **37** 151 (2011)
71. Ledentsov L S, Somov B V*Astron. Lett.* **37** 744 (2012); *Pis'ma Astron. Zh.* **38** 831 (2012)
72. Somov B V *Fundamentals of Cosmic Electrodynamics* (Dordrecht: Kluwer Acad. Publ., 1994)
73. Akhiezer A I, Lyubarskii G Ya, Polovin R V *Sov. Phys. JETP* **8** 507 (1959); *Zh. Eksp. Teor. Fiz.* **35** 731 (1958)
74. Syrovatskii S I *Sov. Phys. JETP* **8** 1024 (1959); *Zh. Eksp. Teor. Fiz.* **35** 1466 (1958)
75. Roikhvarger Z B, Syrovatskii S I *Sov. Phys. JETP* **39** 654 (1974); *Zh. Eksp. Teor. Fiz.* **66** 1338 (1974)
76. Landau L D, Lifshitz E M *Statistical Physics* Vol. 1 (Oxford: Pegramon Press, 1980); Translated from Russian: *Statisticheskaya Fizika* Vol. 1 (Moscow: Nauka, 1976)
77. Priest E R *Solar Magneto-hydrodynamics* (Dordrecht: D. Reidel Publ. Co., 1982)
78. Priest E, Forbes T *Magnetic Reconnection*: *MHD Theory and Applications* (Cambridge: Cambridge Univ. Press, 2000)
79. Kulsrud R M *Earth Planets Space* **53** 417 (2001)
80. Malyshkin L M, Linde T, Kulsrud R M *Phys. Plasmas* **12** 102902 (2005)
81. Somov B V, Syrovatskii S I *Solar Phys.* **75** 237 (1982)
82. Oreshina A V, Somov B V *Astron. Astrophys.* **331** 1078 (1998)
83. Lazarian A, Vishniac E T, in *Magnetic Fields in the Universe II*: *From Laboratory and Stars to the Primordial Universe* (Revista Mexicana de Astronomía y Astrofisicaû Ser. de Conferencias, Vol. 36, Eds A Esquivel et al.) (Mexico: Instituto de Astronomía, 2009) p. 81
84. Eyink G L, Lazarian A, Vishniac E T *Astrophys. J.* **743** 51 (2011)
85. Somov B V, Syrovatskii S I *Proc. P.N. Lebedev Phys. Inst.* **74** 13 (1976); *Tr. Fiz. Inst. Akad. Nauk SSSR* **74** 14 (1974)
86. Podgornyi A I, Syrovatskii S I *Sov. J. Plasma Phys.* **7** 580 (1981); *Fiz. Plazmy* **7** 1055 (1981)
87. Karpen J T et al. *Astrophys. J.* **495** 491 (1998)
88. Priest E R, Lee L C *J. Plasma Phys.* **44** 337 (1990)
89. Kontorovich V M *Sov. Phys. JETP* **8** 851 (1958); *Zh. Eksp. Teor. Fiz.* **35** 1216 (1958)
90. Anderson J E *Magnetohydrodynamic Shock Wawes* (Cambridge: M.I.T. Press, 1963)
91. Furth H P, Killeen J, Rosenbluth M N *Phys. Fluids* **6** 459 (1963)
92. Somov B V, Verneta A I *Space Sci. Rev.* **65** 253 (1993)
93. Somov B V, Syrovatskii S I *Sov. Phys. JETP* **34** 992 (1972); *Zh. Eksp. Teor. Fiz.* **61** 1864 (1971)
94. Todd L *J. Fluid Mech.* **21** 193 (1965)
95. Markovskii S A, Skorokhodov S L *J. Geophys. Res.* **105** (A6) 12705 (2000)
96. Shibata K *Astrophys. Space Sci.* **264** 129 (1998)